Universidade Federal de Minas Gerais

Master Dissertation

Signs of criticality in a virtual vertebrate retina

Author:
Luisa F. Ramírez

Advisor:
Phd. Ronald Dickman

A thesis submitted in fulfilment of the requirements
for the master of Physics

in the

ICEX-Universidade Federal de Minas Gerais

October 2018

Abstract

Signs of criticality in a virtual vertebrate retina

The objective of our work is to apply the concepts of statistical mechanics to the virtual retina of a vertebrate, in order to verify some of the assertions made in Ref [51]. By means of a whole simulation of the vertebrate retina network[35], we obtained data from the ganglion layer as a discrete pattern of activity (spike), or silence from each ganglion neuron. We used maximum entropy criteria to find the probability distribution that describes the system, and we used inverse Monte Carlo simulations for fitting the parameters to within a precision by means of a gradient descent algorithm. Since our purpose is to make a thermodynamic analysis of this system, we found this distribution for different groups of neurons with sizes ranging from 9 to 49 cells each, and we constructed the curves of specific heat. We found that these curves have a peak increasing with the system length at the effective temperature of the retina, suggesting the existence of criticality. In addition, our results agree with the experiments carried out in Ref [51] and strengthen the hypothesis that biological systems may work in a critical state.

Acknowledgements

I want to thank my parents Angela and Fernando for supporting me both emotionally and economically along my professional career and guiding me in my daily life; I owe them a debt of gratitude. Also, I thank my brother John for supporting me in the difficult moments; he always believed in me and encouraged me to continue forward.

I sincerely thank my advisor Prof. Ronald Dickman for the continuous support of my master study and research, for sharing with me his broad knowledge and keeping me motivated, for his enormous patience and valuable advises. His guidance helped me to find a passionate research area which opened many professional opportunities to me. I could not have imagined having a better advisor and mentor for my Ph.D. study.

My sincere thanks also go to Prof. William Bialek for offering me the opportunity of know in the flesh the experimental and theoretical team who inspired my work and for taking me into account as a potential visitor research student at Princeton University. I thank the ICTP, ICTP-SAIFR, FAPEMIG, SBF and the physics committee for the economic support to attend to schools and conferences, motivating my continuous learning. In addition, I want to thank Mauro Copelli for his observations and suggestions which helped me to improve my simulation methods.

I thank my fellow research mates for the stimulating discussions and the continuous ideas exchange, which helped me to increase and strengthen my knowledge of statistical physics. I thank my mates: Bonnie, Rodrigo, Ronaldo, Edson, Arthur, Ludmila and Wil for the academical discussions and for showing me the Brazilian culture. I thank my friends Juan Pablo, Luis, Adriana, Elvis, Milena, the little Vicky, Adalberto, Thiago, Eduard, Ezequiel, Alix, and Gabriela for supporting me and offering me an invaluable friendship. Finally, I thank my best friends Jennifer and Rafael for the strong support in the most difficult moments through the last two years.

At the end but not least, I thank CNPq for the financial support over my master period. Without their support, I would not have been able to finish my research project and obtain my master degree.

Contents

Dedicated to my mother Angela, my father Fernando and my brother John

Chapter 1

Introduction

Understanding the brain is an issue involving multiple areas of knowledge, such as philosophy and medicine. For example, the famous quote *Cogito ergo sum*, by Descartes[1], evidences the early philosophical interest in topics related with the cognition and consciousness. In contrast with most of the systems studied by humans, such as the human body in medicine or classical mechanics in physics, the brain became a challenge due to the absence of experimental evidence. It is clear, for instance, that the mechanisms of the brain for processing information are not visible to the naked eye. Consequently, neuroscience was born as an interdisciplinary research field, taking concepts from different areas, such as chemistry or physics, for improving experiments and generating new theories. For example, magnetic resonance imaging (MRI) is a useful tool based on the principles of radiation[2], showing the levels of oxygen in the brain and providing a full image of the activity in different regions. This tool is widely used both for medical purposes, such as diagnostics[3], and for scientific purposes, such as the study of human visual[4] or motor[5] cortex.

Microscopically, we could focus on the neurons [1] and, using chemistry and biophysics, understanding their internal behaviour and some of their connections [2]. Nevertheless, the chemical complexity, both of the neuron and its interactions (see chapter chapter 2), makes it impossible to describe the whole brain using this complex framework. On the other hand, we could make some approximations,

[1] The neuron is the fundamental cell of the nervous system, which was first proposed by *Santiago Ramón y Cajal*[6].

[2] These interactions among cells take place on the synapses, which can be of electrical or chemical nature (see chapter 2).

such as assigning a weight[3] to each individual connection, and then, by means of a network structure [7] [8] [9], describing the information flow of the system. Still, the problems remain in the sense that, with this computational framework, we dismiss many details which are biologically relevant.

Therefore, we need to choose an adequate analysis framework, depending on the characteristics of the problem. From the viewpoint of the physics and computational sciences, one of the most important questions would be *How does the brain process enormous quantities of information in an efficient way?* In that sense, we could reduce the brain to a network, searching for an optimal arrangement of information processing. From the viewpoint of biology, for instance, one possible question would be *Why is the brain necessary, and why did it evolve as it did?*. To answer this question, rather than reduce the brain to an information machine, we must include biological, experimental and historical facts to analyse the system and its interactions.

In this work, we will have a computational and physical emphasis in the sense that we will analyse a part of the nervous system as a network, reducing the complex chemical interactions to simpler constant weights. However, it is remarkable that in the network structure, we will take into account many biological details which will allow the comparison of our model with real experiments. Consequently, the purpose of our work is based on, by means of the theory of criticality, proposing ideas for understanding how the brain reaches the optimal information transmission and testing the hypothesis of the *critical brain*[10]. In order to understand the meaning of a *critical state* in the brain, we will introduce both the self organized criticality (SOC) and the Griffiths phases theory, both applied to complex systems and specifically to the brain.

First, we may ask how the concept of information flux in the brain is defined. Biologically, given an external stimulus such as a sound, some specialized neurons are activated, possibly exciting their neighbours, which at the same time excite other cells, and so on. This *avalanche* of excitations is the result of a chain reaction corresponding to a flow of information in the brain. Thus, by looking at the features of these avalanches, we might discover some general features of the brain. The theory of SOC describes this type of phenomena, proposing that the system reaches the critical state naturally[11], based on the study of some natural phenomena and complex systems, such as earthquakes[12] or fractals[13].

[3]The simpler example would be the representation of each interaction by a fixed weight

For a sub-system of approximately 1×10^2 neurons, as these used in our work and real experimental works[51], we can define some general concepts for introducing these theories of criticality. In the SOC framework, depending on the size of the avalanches s in the brain[4] (See figure 1.1), we can identify three regimes describing different situations. First, when the avalanches are small compared with the number of cells, we define the subcritical phase, meaning that the number of cells excited is too small such that its distribution decays exponentially as $\exp(-s/s_0)$, where s_0 is a typical value of the system.

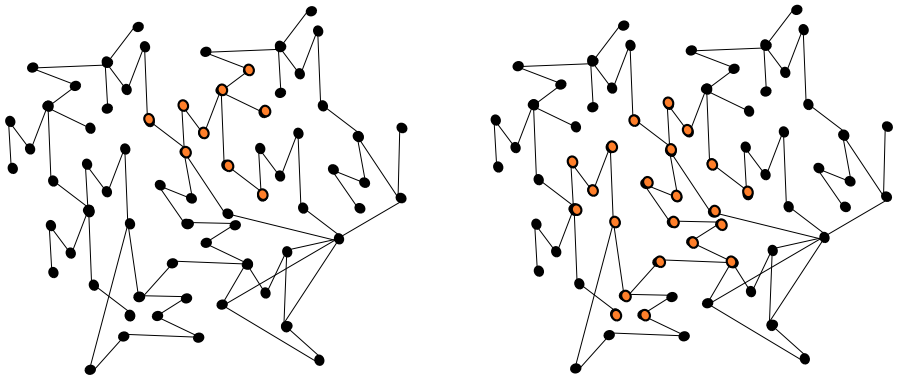

FIGURE 1.1: Sketch of avalanches in a network. The black (orange) points represent the inactive (active) neurons, and the lines the synapses. Left sketch shows an avalanche of size N=9 and right sketch shows an avalanche of N=22.

Second, when the avalanches are compared with the size of the whole system, the phase is known as supercritical, and does not allow the description of its distribution as a power law, in fact, it is possible to obtain just a single large avalanche, meaning that all neurons excite under the same stimulus. Finally, we define the third regime as the critical phase, in which, the distributions of avalanches follows a power law $N(s) \approx s^{-\tau}$, before decaying exponentially for large s. From this viewpoint, the powerful assertion of SOC theory is that the brain operates at this critical point, which is reached by means of an internal control system[5], as in the case of the other complex systems described with SOC[11]. Still,

[4]The size of the avalanche is defined with the number of neurons excited under the same initial stimulus.

[5]For keeping the system at the critical point, there is a kind of control system forcing the system to keep that state without the intervention of external forces. The toy model of SOC is the sandpile which, at the critical point, generates avalanches of different sizes described by a power law. The phase transition of this system is to an *absorbing state*.

the natural question is *Whether this tuning exist, and how is it produced?* and beyond, *Is it true that the brain operates at only one critical point?*.

The second approach is based on Griffiths phases [14], where the system reaches the critical state because of the disordered nature of the network, instead of a control system, as in the case of SOC. In addition, in this case the system exhibits criticality in a broad region, in contrast with the SOC theory, where the criticality is reached only in a point. Therefore, using this theory in the brain, we do not need to find any physical feature forcing the system to the critical region, and we do not need to assume that the brain is always in the same state, due to its broad critical region. Here, the questions for answering are related with the physical structure in the brain, for instance, *Are the empirical reported power-laws strongly related to the disordered nature of the networks?* [15].

So far, we talked about the criticality of complex systems without making any assumption about its equilibrium or non-equilibrium nature. Nevertheless, by using equilibrium statistical mechanics we could analyse the criticality of the system, looking at the behaviour of some physical properties, such as the specific heat [16]. In this work we will focus the analysis of a neuronal network, in our case a retinal network, proposing a thermodynamics by means of the information theory and the maximum entropy model.

This dissertation is divided in three chapters. The first will be focused on the biological and computational study of the retina. Then, we will discuss the biological and anatomical features of the system in order to compare with the simulations. The second will be dedicated to the study of statistical mechanics and maximum entropy model, and finally, the third chapter will be dedicated to the discussion and analysis of our results.

Chapter 2

Biological and computational study of the retina

2.1 Basic structures

The brain is a complex structure composed of about 10^{11} neurons, which are connected between them by around of 10^{15} synapses [17]. Given its complexity and importance, explaining and understanding the behaviour of this system has been the goal of several research areas. For example, from a medical viewpoint, the study of this structure helps to understand some processes responsible for important daily tasks, generating or improving some treatments for neuronal diseases. From a computational viewpoint, this complex structure is studied as an optimized machine processing a huge quantity of information in a short time, aiming for improving technological devices and increasing the efficiency of complex computational tasks.

In this chapter, we will explore first the microscopical structure of the brain, focusing on its basic cells and structures. In addition, we will study how the electrical impulses are generated after applying an external stimulus, and how they propagate throughout the brain. Finally, we will make both a biological and a computational study of the retina.

2.1.1 Neurons and glial cells

Neurons and glial cells determine the behaviour of the central nervous system (CNS), which contains the brain and the spinal cord [18]. Given that there are a lot of sub-structures with different tasks into the CNS, there are several types of cells with different anatomical properties.

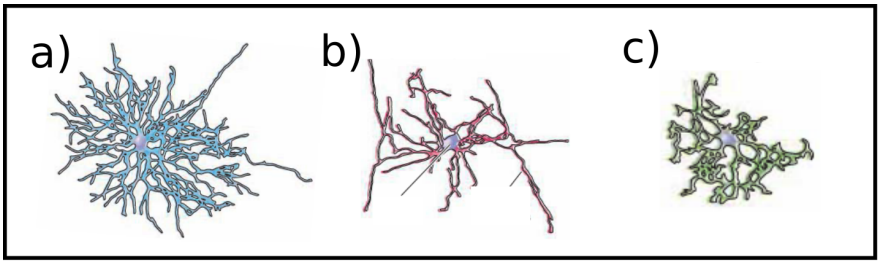

FIGURE 2.1: Glial cells. a) Atrocyte. b) Oligodendrocyte. c) Microglial cell. Figure modified from [17]

Glial cells re located over all the CNS, complementing the work of neurons and increasing their efficiency in signal propagation. As is shown in figure 2.1, there are three types of glias whose differences lie in anatomical and functional aspects. The Astrocytes have a star-like appearance and are in charge of keeping an appropriate chemical environment at the synapses, which means that, they remove ions and molecules which could modify the resting potential. The Oligodendrocytes are just found in some parts of the CNS, wrapping myelin around the axons of neurons, increasing the mean speed of the impulse transmission. Finally, the Microglial cells are in charge of cleaning up dead tissue and replacing it. Hence, after a neuronal injury, the affected part of the brain is filled by these cells, becoming an *inactive* zone [1].

[1]The glial cells are incapable of generating the same connections and electrical impulses as the neurons.

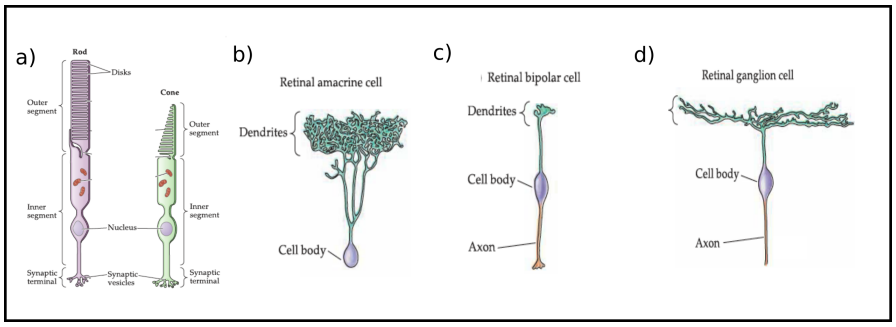

FIGURE 2.2: Some types of neuronal cells. a) Photoreceptors. b) Amacrine cell. c) Bipolar cell. d) Ganglion cell. Figure modified from [17]

The neurons are the cells responsible for the transmission of electrical impulses throughout the CNS. In general, they consist of the soma, in which the main structures such as the nucleus and some organelles are found, the dendrites, which are the ramifications receiving stimuli from other cells or the environment, and finally the axon, which is the ramification transmitting the response to other cells. Nevertheless, not all neurons possess an axon[19].

Different types of neurons are categorized by anatomical aspects, such as number of axons or dendrites, which generally are grouped in specific areas of the CNS. Figure 2.2 shows some of the neurons found in the retina. (The retinal amacrine cell has no axon).

Besides their anatomical properties, neurons have chemical and electric properties, defining other important concepts in the understanding of stimuli propagation. As is shown in the sketch on the left side of figure 2.3, cells contain several species of positive and negative ions, which diffuse across the membrane reaching an electro-chemical equilibrium [17], and generating a potential difference between the extracellular and intracellular environments. This ionic circulation is possible because of the ion channels, which are structures formed in the cellular membrane, allowing ions to enter or leave the cell.

2.1.1.1 Synapses

When an external stimulus is received by specialized neurons, it is transformed into electrical signals which are propagated across the CNS. This propagation

is possible because of *bridges* between neurons, *synapses*, which connect a pre-synaptic and a post-synaptic cell. These connections can be classified into chemical (with a cleft[2]), and electrical (directly connected) (see right sketch of figure 2.3).

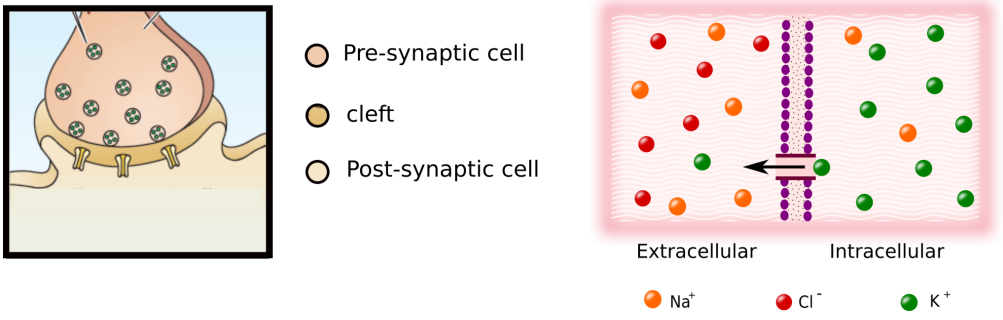

FIGURE 2.3: b) Synapse structure, pre-synaptic cell release neurotransmitters into the cleft which activates the ion channels to allow the ions flowing through cell. a) Electrochemical equilibrium among intracellular and extracellular environment.

In chemical synapses, the pre-synaptic and post-synaptic cells are not in direct contact, rather, when a pre-synaptic cell is stimulated so that reaches its threshold, the propagated signal produces a potential difference, increasing the permeability of the membrane to positive ions, such as Na^+. These ions activate some vesicles leading to release of neurotransmitters[3] into the cleft. The post-synaptic cells possess ion channels or structures with sensibility to neurotransmitters, thus when released into the cleft, ions begin to flow through the post-synaptic cell membrane, changing its potential difference.

Therefore, when a spike[4] is generated in a neuron, it may propagate by means of synapses. In general, neurons can create or destroy synapses depending on the stimulation frequency. This property is called plasticity and makes learning possible.

2.1.1.2 Hodgkin & Huxley model of neurons

For understanding in a more detailed way the biophysics of synapses, we will describe briefly the mechanisms used by the neurons to achieve signal transmission

[2]Synaptic space between pre-synaptic and post-synaptic cells.
[3]Chemical signals which act as messengers in the action potential propagation.
[4]electrical signal that travels along the axons of the neurons for propagating.

and we will introduce the famous model of Hodgkin & Huxley[20], describing quantitatively these complex processes.

Following the previous discussion, we know that the neurons are quite sensitive to changes in their membrane potential, generating ion fluxes across the membrane. Within the cellular membrane of each neuron, there are many types of *channels* (made up of protein) which, depending on the kind of stimuli, allowing the hyper-polarization or depolarization of the cell[5]. Thus, depending on the region in the membrane, it is possible to find channels activated by neurotransmitters, electrical fluxes or mechanical pressure. For instance, in a chemical synapse, when a spikel is generated in the pre-synaptic cell, a certain neurotransmitter, such as glutamate or GABA, is released into the cleft, activating these proteins[17].

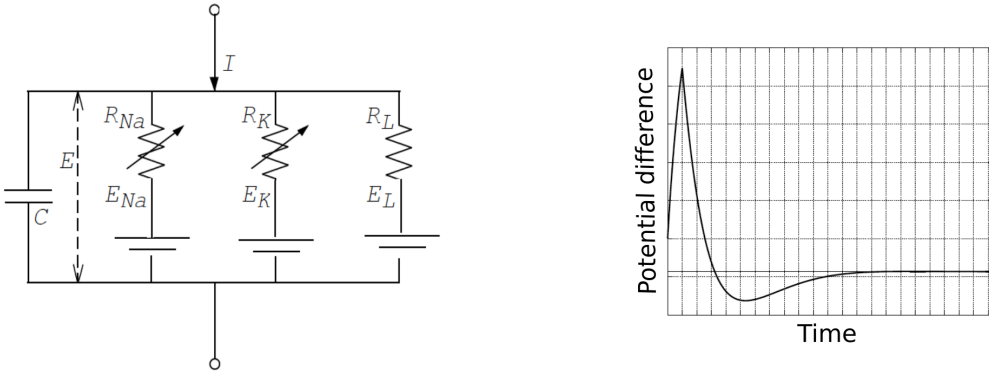

FIGURE 2.4: Hodgkin & Huxley model. a) Sketch of the circuit representing the neuron. b) Graph of the potential difference within the cellular membrane of a neuron during a spike.

These ionic channels are responsible for selecting different types of ions and allowing them to enter or leave the cell. Consequently, depending on the electric field of the ions[21], the channel selects and dehydrates them, allowing them to flow across the membrane. In general, in a synapses there are many types of ion channels for mediating the flow of all the ions participating in the propagation of the spike. Nevertheless, from a general viewpoint, some of them contribute with a stronger weight to the cell polarization, for that reason, in the quantitative model

[5]Without the effects of external stimuli, each neuron has a resting potential (normally, -70mV) in which, both the chemical and electrical forces equilibrate. When a current travels across the membrane decreassing (increassing) this potential, we say that the cell is hypolarized (depolarized).

some of these weak ion currents, such as the Ca^{+2} current, are described as a leakage current of the membrane.

As is shown in the left sketch of figure 2.4, the neuron can be modelled as a RC circuit, where each resistance describes the ion channels. By analysing the circuit, we obtain the voltage differential equation:

$$\begin{aligned} C\frac{dV}{dt} &= I - g_k n^4(V - E_K) - g_{Na} m^3 h(V - E_{Na}) - g_l(V - E_l) \qquad (2.1) \\ \frac{dn}{dt} &= \alpha_n(V)(1 - n) - \beta_n(V)n \\ \frac{dm}{dt} &= \alpha_m(V)(1 - m) - \beta_m(V)m \\ \frac{dh}{dt} &= \alpha_h(V)(1 - h) - \beta_h(V)h \end{aligned}$$

The variables n, m and h describe and model the behaviour of the Potassium and Sodium ion channels based on experimental observations (For more experimental details, see the original paper [20]). The right graph of figure 2.4 shows the potential difference of the membrane when spiking. First the cell depolarizes to reach its threshold, in which its activity maximizes for reaching its maximum potential value. After, in order to reach its electrochemical equilibrium, the cell becomes hyperpolarized during a refractory period, in which, independently of the external stimuli, the cell does not exhibit any response. This electro-physical behaviour is fully observed in experimental works[22] and quantitatively described by this set of differential equations.

2.2 Visual system

The visual process can be divided into three parts: image focusing, retinal processing and cortical processing (see figure 2.5). The first takes place in the eye and has the function of focusing the image on a region of the retina[6] as sharply as possible. The complexity of this task lies in the fact that the stimuli emerge from

[6]In primates, this region is known as fovea and contains the highest density of cones

different sources having different luminosity, contrast and depth. Consequently, depending on the stimuli features, some internal structures, such as the lens or the pupil, are activated[17] focusing the images on the retina.

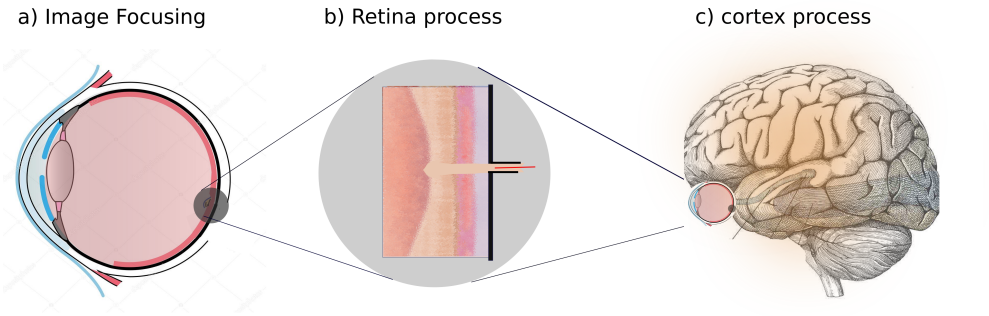

FIGURE 2.5: Sight process. a) Image focusing process which happens in the eye and finish at retina. b) Shows the retina process which starts with the focused image and finish with a response at ganglia layer. c) Shows the cortex process which generates the final response.

The second process involves the retina, which is in charge of transforming the light signal into an electrical response which is sent to the cortex. Finally, this signal is processed in some areas of the brain, such as the lateral geniculate nucleus and the visual cortex, generating a final response. Given that our work is based on the retina, the next section will be dedicated to the study of this system and its biological processes.

2.2.1 Retina

From a macroscopic viewpoint, the vertebrate retina is a membrane located at the back of eye, including a high acuity region called the fovea[17][21], and an optic disk, where nerves, arteries and veins enter and/or leave the eye. As was described in the last section, its function is based on the treatment and transformation of luminous signals into electrical impulses, requiring specialized biological processes.

The retina is composed of essentially five kinds of neurons, whose signal transmission is oriented in a vertical way and sent to the cortex via the optic nerve. From a functional point of view, this structure can be divided in the outer and inner retina (see left panel of figure 2.6); both can be further divided into layers.

2.2.1.1 Outer retina

The outer retina contains the neurons and synapses involved in the transformation of the luminous stimuli into electrical signals. Its first layer is composed of photoreceptor cells, which are in charge of the phototransduction process[7], and which can be divided, for mammals, into rods and cones. In contrast with rods, the cones have a slow response to changes in light intensity; the full set of cones have a high spatial resolution. In addition, the majority of cones are situated at the fovea (high acuity region), while rods predominate in the peripheral region.

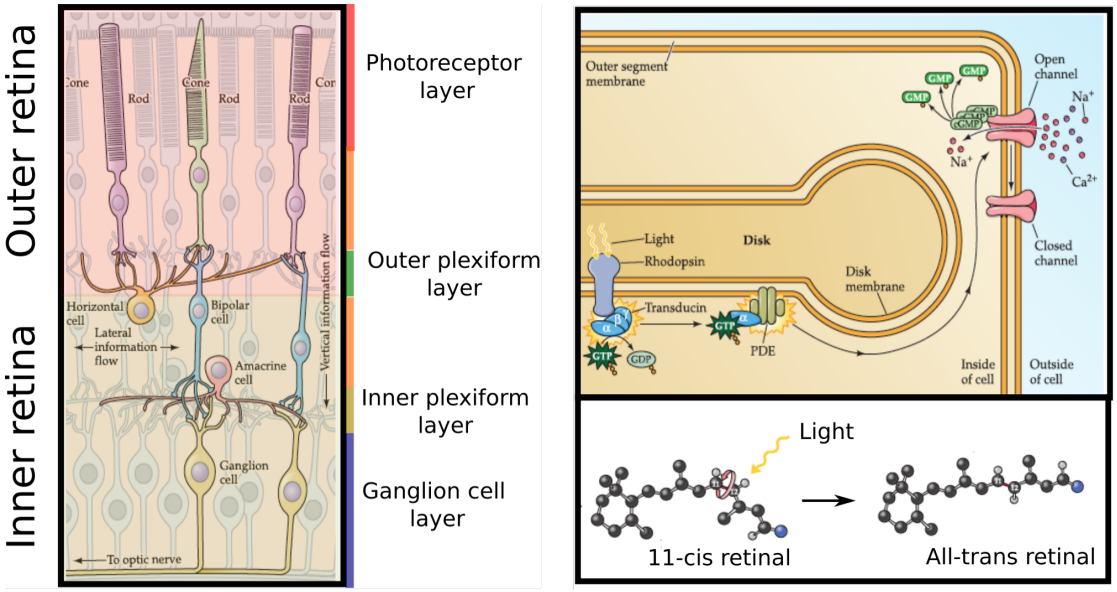

FIGURE 2.6: Left Panel: Retina structure and layers. Right panel: phototransduction process and protein transformation. Figure modified from [17]

In contrast with the cones, the phototransduction process of the rods is well understood, leading to a detailed description of the internal processes generating the first electrical signal. Therefore, we will focus on the anatomy of these cells, in order to describe their interaction with light. In general, these photoreceptors have a body with a rod-like shape, whose first part is composed of disks having contact with the epithelium[8], where the photons arrive. Within the membrane of this disk we find rhodopsin, containing seven transmembrane Opsin and 11-cis

[7]Chemical process changing the potential difference of the membrane cell, because of the interaction with photons.

[8]This structure cover the retina surface, receiving the light beams and controlling the intensity saturation preventing the damage of the photoreceptor cells.

retinal (figure 2.6). Moving inward from the disks, we find the nucleus and the synaptic terminals, where the electrical signal is transmitted.

When photons interact with rhodopsin, 11-cis retinal changes its molecular conformation to All-trans retinal, activating transducin and other second messengers. By means of a chain reaction within the membrane, the Ca^{+2} and Na^{+} channels close, generating an ion flux which leads to the hyperpolarization of the cell[17]. In contrast with most of the neurons in the nervous system, the photoreceptor cells have a continuous and modulated change of their membrane potential, leading to the absence of action potentials or *spikes*. Finally, it is important to highlight that in a luminous environment, both the cellular activity and the ionic flux *decrease*, because of the high rate of photon capture.

Following the phototransduction process, electrical fluxes travel across the axons of photoreceptor cells, activating several synapses with horizontal and bipolar cells. As shown in figure 2.6, the dendrites of horizontal cells make synapses with several photoreceptor axons, connecting them horizontally providing information about the neighbours. The main function of these cells is to process information about the luminance[23] of the stimuli in a broad region of the retina. For instance, one horizontal cell is connected with several photoreceptor cells, providing them a feedback with the mean luminance of the region. Consequently, from a broad viewpoint, the purpose of these connections would be to reduce noise and to smooth the signal from the first layer[24]. Nevertheless, it is believed that this is neither their unique nor their main function. For instance, it has been found that the photoreceptor cells have gap-junction synapses between them[25], opening the possibility of correcting errors before connecting to horizontal cells.

2.2.1.2 Inner retina

Heading inward from the horizontal cells, we next find the bipolar cells, which can be classified into two types: ON and OFF cells. The main purpose of this difference in the retina, is the differentiation of the luminosity of stimuli. For instance, when a bright stimulus is sent to the bipolar layer, the ON cells depolarize while the OFF cells hyperpolarize, creating different paths for signal transmission. As is shown in figure 2.7, all bipolar cells contain both a center and a surround region, allowing the identification of image contrast by means of a modulated change in the membrane potential, meaning that, the intensity of the cell excitation is proportional to the

quantity of luminosity (darkness) in the center of the ON (OFF) cell. Because of this, it is believed that most of the edge enhancement processing take place in this layer, helping to the identification of shapes in the figures in the cortex.

Below the bipolar cells, we find the Amacrine cells, which are located in a horizontal arrangement, connecting several bipolar cells. Their dendritic ramifications are located in different parts of the retina depending on their functionality, dividing this region into two sub-layers: a and b. Therefore, some works[26] claim that this division depends on the type of bipolar cell (ON or OFF) being connected, such that, ON cells would be located in the sub-layer a, while OFF cells would be located in the sub-layer b. Other works[27] relate this division with the functionality of these cells, such as, their sensibility to color differences. In general, amacrine cells have a similar function to horizontal cells, in the sense that they connect several bipolar cells, generating a kind of spatial integration. For instance, when a bipolar cell produces an electrical response, the synapses with the amacrine cells may inhibit it, based on the information of neighbouring bipolar cells.

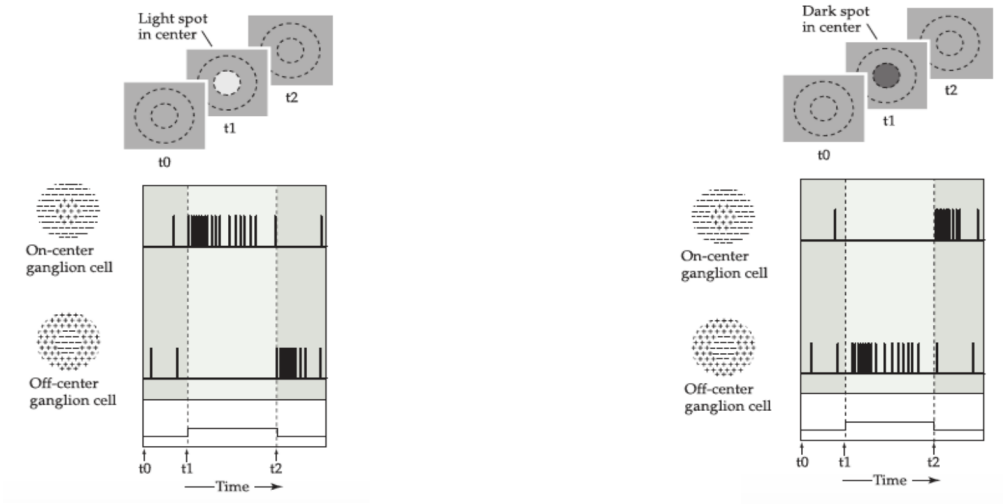

FIGURE 2.7: Potential difference of ON and OFF ganglion cells. Left panel: Bright stimulus in the center filed. Right panel: Dark stimulus in the center. Taken from [17]

The innermost layer of the retina contains the ganglion cells, whose axons compose the optic nerve, carrying information to the brain. Like bipolar cells, these cells have the ON and OFF classification, and are further divided into various types, depending on the species being studied. For instance, the retinal ganglion cells of

cats are sorted into two types labelled X and Y, whose difference lies in the type of cells from which they receive input. On the other hand, the retinal ganglion cells of primates are sorted into two types labelled P and M, whose classification depends both on the retinal subnetworks providing the input and their contrast sensitivity [28] [29].

Figure 2.8 presents the most important results of experimental studies of the cat retina[30]. The stimulus used was a grey-scale sinusoidal pattern, varying along the center-region of the ganglion cell. In this set up, the experiments changed the location of the pattern with respect to the receptive field center of each cell, and they changed its phase, measuring the response of the ganglion cells. As expected, they found first the behavioural difference between ON and OFF cells, observing the excitation intensity in each case. Afterward, by comparing different OFF-cells, they found another difference in their behaviour, depending on the symmetric distribution (or phase) of the stimulus. For instance, the odd experiments (90^o and 270^o) showed in the figure, revealed a strong difference between cell types: while the first does not have response, the second shows activity when the stimulus enters and leaves the center region.

Therefore, according to the distribution of the stimuli, we must take into account four types of ganglion cells in the cat retina: X-ON, Y-ON, X-OFF and Y-OFF cells. In the case of other mammals such as primates, the responses vary depending on other features of the stimulus, generating a totally different is classification.

Based on this biological description of the retina, we will use the next sections for describing our simulation and, with the aim of proving its feasibility, we will contrast some of the simulated results with real retina data.

2.3 Virtual vertebrate retina

In some works [31] [32] [33] [34], the retina has been studied as a network, in which the input is given by the luminous stimulus, the nodes by neurons and the links by synapses. The differences among these works lie in their computational structure, such that there are some simulations taking into account several biological details, preserving with high fidelity the anatomical arrangement of cells, in contrast with

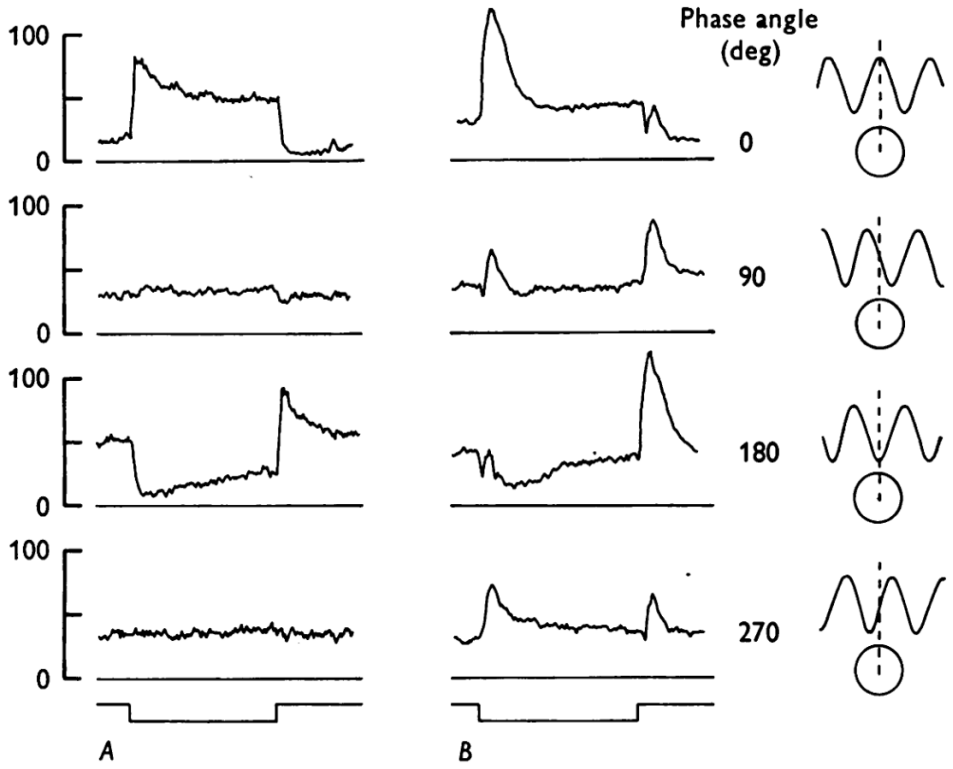

FIGURE 2.8: Responses of an off-center X-cell (A) and an off-center Y-cell (B) to the introduction and withdrawal of a stationary sinusoidal grating pattern. Taken from [30]

others that ignore some biological details, but have greater higher computational efficiency.

In this section we will introduce the virtual retina software [35], which was used in our work as the retina simulator. We will describe its network structure by comparing with the real vertebrate retina. Finally, using the previous study about the vertebrate retina, we will discuss the most relevant biological details for taking into account in our work.

2.3.1 Stimuli

For terrestrial mammals as primates, a common scene could be many primates eating fresh fruits in the wild, while for aquatic animals, it could be that of a group of fish swimming around aquatic plants. Thus, depending on the species that we are studying, we should use a stimulus similar to its natural environment.

As we will study in the next subsections, we will use the features of a mammalian retina with some specific aspects of the human and cat retinas. Thus, the stimuli used in our simulations represent what would be natural scenes for these species (see chapter 4).

The film $L(x, y, t)$ is constructed as a set of static correlated images in grey-scale, such that, each one is sent to the first layer of the virtual retina (VR) and maintained for a short time before being replaced by the next. Each image is represented as a matrix of pixels, where each site represents the light intensity of the region ranging from 0 to 255.

Following the same structure used for describing the vertebrate retina, we will divide the virtual retina in layers, starting with the outer retina, continuing with the inner retina and ending with the ganglion layer. In addition, in the following subsections we will use the spatial and temporal filters described in Appendix A, in order to simulate the biological process of the retina.

2.3.2 Outer virtual retina

The mathematical model of the photoreceptor layer takes into account the temporal features of the phototransduction process and the spatial features of the gap junctions among photoreceptor cells. Thus, taking into account the complexity of this process, the temporal evolution is modelled as a partially transient linear cascade, starting with an exponential cascade filter $E_{n_c,\tau_c}(t)$ and followed by a partially transient filter $T_{\omega,\tau}$. It is important to remark that this filter is valid only for stimuli with a smooth variation in intensity. With respect to the spatial filter, a Gaussian filter G_{σ_c} is used describing the connections among rods, so that we can write the final response of the photoreceptor layer $C(x, y, t)$ as:

$$
\begin{aligned}
C(x,y,t) &= G_{\sigma_c} * T_{\omega,\tau} * E_{n_c,\tau_c}(t) * L(x,y,t) \\
E_{n_c,\tau c}(t) &= (n_c t)^{n_c} \frac{exp(\frac{-n_c t}{\tau})}{(n_c-1)!\,\tau_c^{n_c+1}} \\
T_{\omega,\tau}(t) &= \delta_0(t) - \omega E_\tau(t) \\
G_{\sigma_c}(x,y) &= \frac{exp(-\frac{x^2+y^2}{2\sigma_c^2})}{2\pi\sigma_c}
\end{aligned}
\tag{2.2}
$$

Both spatial and temporal filters are introduced as convolutions ($*$) over the original stimuli. In addition, each filter has a set of characteristic parameters which are setted based on biological facts or experimental observations (See Appendix A).

After the photoreceptor processing, the signal $C(x,y,t)$ passes to the horizontal layer, whose temporal response is modelled by an exponential filter $E_{\tau_c}(t)$, describing the temporal characteristics of synaptic transmission in the synapses. In addition, as we studied in the biological structure, these cells have a wide spatial connection which is described by another Gaussian filter G_{σ_s} whose variance σ_s is greater than the central variance σ_c. Consequently, we have the mathematical description:

$$
\begin{aligned}
S(x,y,t) &= G_{\sigma_s} * E_{\tau_s}(t) * C(x,y,t) \\
E_{\tau_s}(t) &= \frac{exp(\frac{-t}{\tau_s)}}{\tau_s}
\end{aligned}
\tag{2.3}
$$

Both the photoreceptor and horizontal layers can be seen as a *center-surround* system; outer plexiform layer (OPL), in the sense that signals from photoreceptor cells provide a high acuity, in a narrow region, while signals from horizontal cells perform spatial integration of several cells, inhibiting the primary responses of photoreceptor cells. Mathematically, this final current of the OPL I_{OPL} is expressed as a signal of the center field corrected by a signal from the surroundings,

$$
I_{OPL}(x,y,t) = \lambda_{OPL}(C(x,y,t) - \omega_{OPL} S(x,y,t)), \tag{2.4}
$$

where λ_{OPL} is an overall gain and ω_{OPL} is a relative weight between the two signals.

2.3.3 Inner retina

Based on the biological discussion about the inner retina, we can attribute most of the contrast process to this layer, and consequently, regard contrast gain control[9] as a process taking place in this region via amacrine cells or leakage currents, and which can be mathematically modelled as a set of non-linear equations2.5-2.7. In this section we will focus on this important aspect of the visual system, reducing the virtual inner plexiform layer (IPL) to this non-linear process described by:

$$\frac{dV_{bip}}{dt} = I_{OPL}(x,y,t) - g_A(x,y,t)V_{bip}(x,y,t) \quad (2.5)$$

$$g_A(x,y,t) = G_{\sigma_A} * E_{\tau_A} * Q(V_{bip})(x,y,t) \quad (2.6)$$

$$Q(V_{bip}) = g_A^0 + \lambda_A V_{bip}^2, \quad (2.7)$$

where g_A represents the leakage conductance. Looking at Equation A.1, we have that each leaky ion channel in the membrane contributes two current terms: the Nernst equilibrium potential and the leakage current, depending directly on V_{bip}. In the Hodking & Huxley approach, we neglect the second term for simplicity. Nevertheless, taking into account that the phenomenon that we are trying to describe is probably mediated by this leakage current, we must consider it in our equations.

So far, we have equation 2.5, describing the currents flowing across the ion channels[20] (see Appendix A), with the difference that here, the leakage conductance depends on V_{bip} via $Q_{V_{bip}}$. In contrast with the leakage currents explanation, other theories claim that these currents are generated by amacrine cells as a feedback signal. In both cases, this processing has both an integration time which is represented by the exponential filter E_{τ_A}, and a spatial resolution described with the Gaussian spatial filter G_{σ_A}. This spatial resolution is generated

[9] This phenomenon describes and explains the changes in the processing of images with different contrast. For instance, there are studies[36] showing the difference of the perception of an image with different background contrasts. Adaptation to contrast changes is a biological relevant process to be considered in simulations.

by gap junctions among bipolar cells or by the dentritic ramifications of amacrine cells. Nonetheless, there is no direct biological comparison to fix the characteristic parameters τ and σ of these filters; they are fixed by fitting the model to experimental results.

An important fact about the virtual inner retina is that, in contrast with the real inner retina, the signal is not split into ON and OFF paths. The justification is that although the processing within the virtual inner retina maintains the symmetry between hyperpolarized and depolarized regimes, this splitting can be made in the virtual ganglion layer. Consequently, the first constraint on $Q_{V_{bip}}$ is that it must be even with respect to a change in the sign of V_{bip}, in order to include the contrast effects in both types of cells. In addition, for reproducing some experimental observations, it was found necessary to use a function that is constant in the vicinity of $V_{bip} = 0$. The simplest mathematical expression satisfying these conditions is given in Eq.2.7.

Summarizing, the set of equations 2.5-2.7 describes the variation of the bipolar membrane potential in time, depending on the primary current from the outer plexiform layer $I_{OPL}(x, y, t)$ and the conductance term $g_A(x, y, t)$, which at the same time depends on the spatial and temporal filtering function QV_{bip}. In addition, for biological and experimental convenience, the functional form of $Q(V_{bip})$ is fixed as a symmetric and convex function describing both the inert leaks in the membrane and the non-linear dependence on the potential V_{bip}. The λ_A term controls the strength of the gain control feedback loop.

2.3.4 Ganglion layer

In this section, we will discuss the final processing of the electrical signal and the model used for discretizing the response. In addition, we will include some functional differences of neurons, such as their ON and OFF nature, by means of some mathematical differences in their model. The mathematical treatment of this layer does not describe individually all the biological details, rather, it has a functional emphasis aiming for describing, in a general way, experimental observations on real retinas.

Given that the difference between the ON and OFF cells lies in the opposite response of their ionic channels, which depolarize or hyperpolarize respectively

with a luminous stimulus. It is possible to describe them by setting the parameter $\epsilon = 1, -1$ in the membrane potential, supposing that the strengths of the two responses are equal. In addition, we must consider the difference among Y and X ganglion cells, whose main difference lies in their integration time; X cells are tonic while Y cells are phasic[10]. Thus, for describing them, a transient temporal filter T_{ω_G,τ_G} is used with a different weight transient ω_G, such that for X cells $\omega_G = 0.7$ and for Y cells $\omega_G = 1$.

In addition, the virtual ganglion layer contains a rectification function, taking into account some non-linearities (see below) produced by saturation or synaptic transmission, given by:

$$N(V) = \begin{cases} \frac{i_G^0}{1-\lambda_G(V-v_G^0)/i_g^0} & if \quad V < v_G^0 \\ \\ i_G^0 + \lambda_G(V - v_G^0) & if \quad V > v_G^0 \end{cases}$$

Where v_G^0 is the linearity threshold, where the response of the transmission becomes linear. The terms λ_G and i_G^0 have units of *reduced currents* measured in Hertz(see Appendix A). A deeper biological and computational justification for this rectification function is found in [35] [37][38]. Finally, because of the dendritic ramifications of the ganglion cells, the signal passes by a spatial filter G_{σ_G}. Consequently, taking into account all the details, the final current produced by the ganglion cells would be given by:

$$I_G(x, y, t) = G_{\sigma_G} * N(\epsilon T_{\omega_G,\tau_G} * V_{bip}(x, y, t)) \tag{2.8}$$

The hierarchy of the terms in this equation is the same as in the preceding discussion, following the biological chain of events. Nevertheless, some terms are ordered for convenience, for instance, the rectification function is placed after the transient term, given that comparisons with real experiments are more accurate in that way.

By means of the non-linear Integrate and Fire model the signal is discretized, following the rules:

- $\frac{dV_n}{dt} = I_G(x_n, y_n, t) - g^L V_n(t) + \eta_v(t)$,

[10] A tonic process continues for some time after being initiated, while a phasic process shuts down quickly.

- Spike when threshold is reached: $V_n(t_{spike}) = 1$,
- Refractory period: $V_n(t) = 0$ while $t < t_{spike} + \eta_{refractory}$,
- Repeat.

Therefore, in accord with the biophysical behaviour of the neuron (see subsubsection 2.1.1.2), the variation of the potential difference of the membrane depends on the external current and the conductance of the ion channels. In contrast with the Hodgkin & Huxley equation (2.1), here we have an additional term $\eta_v(t)$, adding noise to the model and allowing the reproduction of more realistic and complex experiments (see below). In addition, we know that each cell has a threshold at which it generates a spike; the model simulates this behaviour by setting $V_n(t_{spike}) = 1$ when the potential reaches the threshold[11]. The model includes a refractory period after the spike, during which the cell do not respond to external stimuli.

In order to improve the predictions of the model, a noisy term η_{ref} is added by following a normal law $\mathcal{N}(3ms, 1ms)$[39]. Finally, depending on the type of retina studied, i.e., with or without fovea, the cells must follow the correct spatial distribution. Therefore, the virtual retina can be set up with a uniform distribution of cells, or with distribution

$$s(r) = \begin{cases} 1 & if \quad r < R_0 \\ \\ 1/(1 + K(r - R_0)) & if \quad r > R_0. \end{cases}$$

In the equation above, R_0 represents the size of the fovea and K the rate of density decrease outside it. The justification for choosing this functional form is that the dendritic trees for primate ganglion cells scale in a similar way[40].

The discretized signal generated by the ganglion layer carries the final response of the retina to the brain, by means of the optic nerve composed of ganglion axons. In the next section we will show some of the experimental comparisons made with this simulator in order to validate its similarity to the real vertebrate retina.

[11] In the simulation this parameter was adjusted following the experimental observations.

2.4 Comparison with experiment

2.4.1 X and Y ganglion cells

The first experiment made with the simulator was the reproduction of the behaviour of X and Y cells under a grating stimulus. The parameters of the spatial filters σ_c and σ_S were the same as measured in the original experimental work[30], while the other parameters were adjusted to fit the observations.

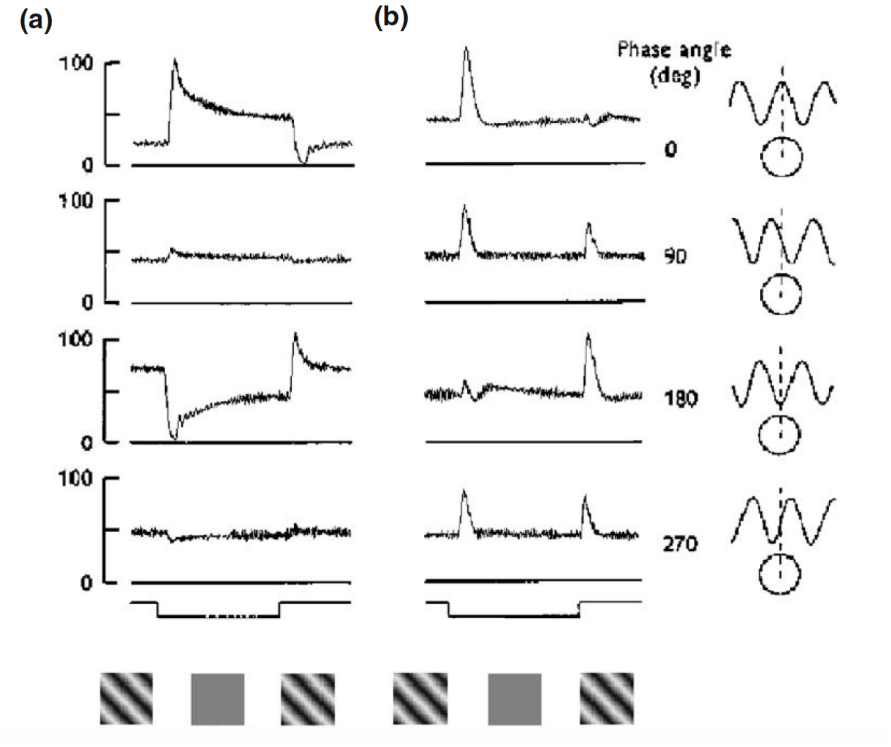

FIGURE 2.9: Reproduction of the responses of an off-center X-cell (A) and an off-center Y-cell (B) to the introduction and withdrawal of a stationary sinusoidal grating pattern. Taken from [35]

Figure 2.9 shows the results obtained with the simulator. First, the curves reproduce the phasic and tonic behaviour of these cells and in addition capture the non-response of X cells under stimuli with a phase angle of 90 and 270 degrees. The reproduction of this behaviour is a consequence of the hierarchy used in equation 2.8, such that the permutation of any term leads to a marked change in the behaviour of the cells. In addition, the use of slow and fast transients $T_{\omega,\tau}$ leads

to the correct reproduction of the tonic behaviour of X cells. Fore additional experimental comparisons see the original paper [35].

In summary, we have presented a detailed study of the neurons and synapses, by showing their anatomical composition and their biophysical behaviour, introducing the Hodgkin & Huxley model as a quantitative description. In addition, we studied specifically the retina, describing its layered structure and the types of neurons found in each layer. In order to understand the processing chain of the retina, we studied the behaviour and functionality of each type of neuron and their connections within the retinal circuit. Finally, we introduced the Virtual retina simulator, which reproduces most of the behaviour observed in real vertebrate retinas. By means of comparisons with the previous biological study, we discussed the mathematical treatment of this network simulation and justified it. Finally, to show that the simulator was able to reproduce important features of this system and validating this software as a feasible simulator of real retinas, we showed both the measurements obtained with the virtual retina and the real retina of a cat, in the ganglion layer under a grating stimulus. We conclude that the results were quite similar and that the most important details were captured by the simulator.

Chapter 3

Information Theory and Statistical Mechanics

The study of complex systems [41] represents a challenge due to the number of parameters which must be taken into account to describe them. An exact mathematical treatment would demand knowledge about all degrees of freedom of each element, becoming an imposible task for systems of many particles and complex interactions. Using statistical mechanics, it is possible to define some physical macroscopic concepts such as temperature and entropy, under the assumption of thermodynamic equilibrium. Nevertheless, this condition is rarely satisfied in real systems, and thus, it is necessary to use other theories to analyse them. Currently, there exists a strong research field, working on the development of a robust theory for non-equilibrium systems [42].

On the other hand, these systems could be studied by using information theory, which is based on probability theory and the information concept which is measured in bits. In that case, there are no physical restrictions on the systems (as the

thermodynamic equilibrium in statistical mechanics), but there are several limitations in the physical interpretations of the results and in their generalization to more complex systems or external conditions. For instance, by using the Shannon entropy we obtain the same mathematical framework as using the thermodynamic entropy, nevertheless we cannot generalize the results obtained to other systems without the physical concepts of temperature or heat, making the results limited compared with the robust theory of thermodynamics. In this chapter we will show that both, statistical mechanics and information theory, have similar mathematical frameworks, which strengthens the idea that, although not known until now, there is a conceptual link among them.

3.1 Statistical mechanics

From a macroscopic point of view, we can use the equation of state to predict the behaviour of some systems in equilibrium, such as the ideal gas or the van der Waals gas [43]. In that way, this behaviour does not depend on microscopic details, such as the velocity and position of each element. Nevertheless, when we are interested in the microscopic details, we must consider all the subsystems, its degrees of freedom and interactions among them. For instance, for the Van der Waals gas, we may consider the degrees of freedom of all the particles and their interactions, which depend on its own composition as the neighbours one.

The microscopic complexity combined with the macroscopic predictable behaviour, inspired the development of statistical mechanics, allowing the study of systems with an enormous number of degrees of freedom and microscopic features, such as the fermions or bosons gas [44]. In addition, in the thermodynamic limit (number of elements going to infinity), the theory matches with the macroscopic predictions, as in the case of the ideal gas.

The main idea of statistical mechanics is to study the systems, as an *ensemble* of subsystems, in the phase space [16]. Depending on the physical features and conditions, it is possible to construct different types of ensembles. For example, whether the energy of the whole system is conserved, we could use the microcanonical ensemble, whether the temperature of the system with a heat bath remains

constant, we could use the canonical ensemble and, in the same way for other physical constrains[45]. In the canonical ensemble, for a system in equilibrium with energy E, the probability distribution corresponds to the Boltzmann distribution:

$$\rho(T) = \frac{e^{-\beta E}}{Z} \tag{3.1}$$

Where $Z = \sum_\zeta e^{-E_\zeta / k_B T}$ is the partition function (ζ corresponding to the state of the system), and $\beta = K_B T$. To complete the review of systems in equilibrium, we must introduce the concept of entropy, which, in the microcanonical ensemble formalism is defined as the logarithm of the number of microstates in the energy surface ($E < H(x) < E_s$) ; with $H(x)$ the Hamiltonian[46][1]:

$$S(E) = \frac{1}{h^{3N}} \int_{E \langle H(x) \langle E+\delta E} d^{6N} x \tag{3.2}$$

Where h is the normalization constant. Thus, with statistical mechanics we can study the properties of any macroscopic system (at equilibrium) with well defined energy, analysing the behaviour of the ensemble, and then, generalizing it to the thermodynamic limit.

On the other hand, statistical mechanics provides a mathematical framework to study phase transitions. In general, a phase transition is defined as a sudden change of a system's properties, as a control parameter such as temperature or pressure is varied. One of the most common examples is the phase transition of a ferromagnetic material into a paramagnetic one, due to the variation of its temperature. This problem can be studied with the Ising model, which was solved precisely in 2-dimensions by Lars Onsager in 1944 [47].

3.2 Ising model, phase transitions and universality for systems at equilibrium

Given the importance of the Ising model in the development and understanding of phase transitions and the universality theory, we use this section to introduce it and show some of its most remarkable results. For a system of N spins arranged

[1] Taken the Boltzmann's constant equal to 1

in a M-dimensional lattice, under the effects of an external magnetic field, we define the microstates using the spin orientation: up or down. These spin variables represent the orientation of the magnetic dipole moment of each element, such that, the configuration space is given by $\sigma = \{\sigma_1, \sigma_2, \cdots, \sigma_N\}$, where each individual spin can take two possible values $\sigma_i = \{-1, 1\}$ (down or up respectively). The Hamiltonian is given by:

$$H = \sum_i h_i \sigma_i + \sum_{ij} J_{ij} \sigma_i \sigma_j \tag{3.3}$$

Where h_i represents the external magnetic field, which in principle can be inhomogeneous, and J_{ij} represents the interaction among spin pairs. To study the phase transition of ferromagnetic material, we consider a d-dimensional lattice, without external magnetic field ($h_i = 0$), and with interactions between first neighbours only[2] (figure 3.1).

Since we have the Hamiltonian, we are able to use the canonical ensemble to calculate the macroscopic properties. The main difference between ferromagnetic and paramagnetic materials lies in the orientation of its spins, such that, in the presence of an external magnetic field, the spins of both materials orient, on average, along the field, but if the field is removed, these orientations are kept only in the ferromagnet.

Therefore, defining the magnetization m [3] as:

$$m = \frac{1}{N} \sum_i \sigma_i \tag{3.4}$$

We obtain that the magnetization is zero for the paramagnetic phase only (see figure 3.1). Consequently, we can use m as the order parameter[4] of the system, with the aim of characterizing the phase transition, such that by looking at the region where the curve presents this sudden change, we can estimate the critical temperature. In figure 3.1 we can observe that in the Ising model the critical

[2]These interactions are the simpler approximation for this problem, reproducing the observed phase transition

[3]Density of magnetic dipole moments

[4]In the study of phase transitions, the order parameter is defined as a quantity which gives information about the symmetry breaking in the system. Normally, it is zero in one phase and different from zero in the other one.

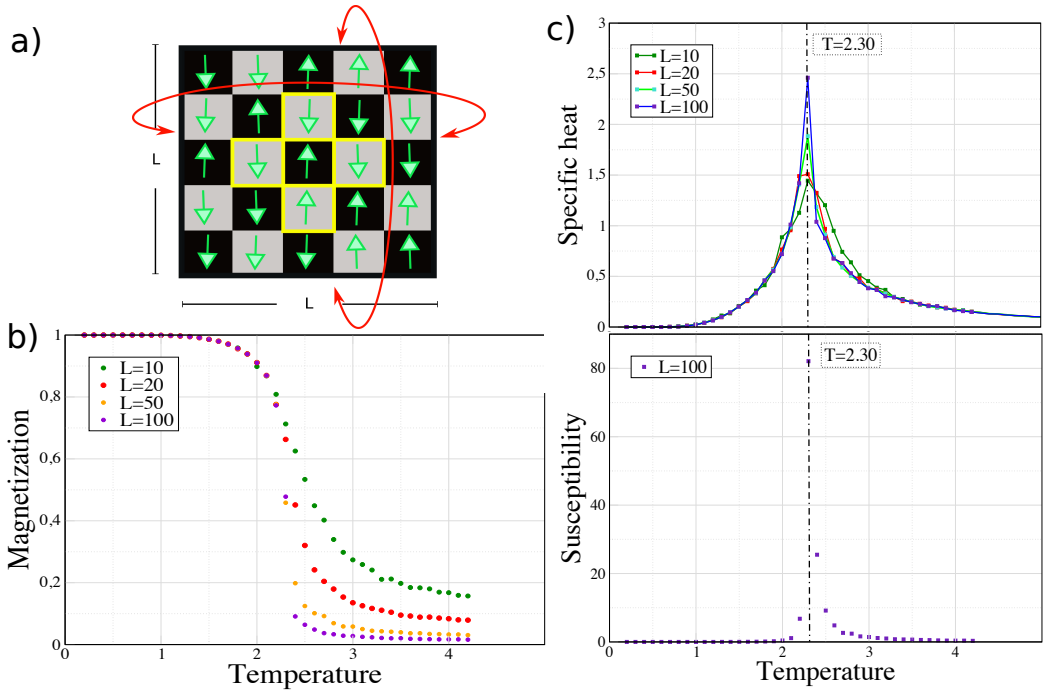

FIGURE 3.1: Two dimensional Ising model on a square lattice with periodic boundaries. a) Sketch of the system; the Yellow region highlights the neighbours of the spin in the middle b) Magnetization curve for different lattice sizes. c) Above: Specific heat curve for different lattice sizes. Below: Susceptibility curve for a lattice of 100 spins.

temperature is located in the interval $(2, 3)$, and that its accuracy improves as the system size increases.

In addition, there are other quantities which behave in a singular manner at the phase transition, such as the specific heat and susceptibility, described by equations 3.5 and 3.6, whose mathematical form involves means over characteristic quantities such as the energy or magnetization. In general, we have that when the system reaches a critical point, these quantities diverge in the thermodynamic limit[5].

$$c \propto Var(E) = \frac{\langle E^2 \rangle - \langle E \rangle^2}{T^2} \tag{3.5}$$

$$\chi \propto Var(m) = \frac{\langle m^2 \rangle - \langle m \rangle^2}{T} \tag{3.6}$$

[5]The divergent behaviour is more dramatic as the system size increases (see figure 3.1).

By looking at the behaviour of these quantities, such as the energy and magnetization in the Ising model, we find that they have local fluctuations appearing at all length scales when the system is at a critical point[48]. For that reason, it is possible to characterize these regions with power laws defined by some critical exponents defining several universality classes. When a system shares the same critical exponents with other systems, we can conclude that its behaviour near of the critical region is similar, leading to a generalization of their properties. Several systems have been successfully studied by using this theory, such as non-equilibrium lattices [49] or statistics of extreme values[50].

3.3 Information Theory

From a different point of view, we can use information theory for modelling many systems by means of the Shannon entropy. First we will define the concept of entropy into the information theory framework and then, we will introduce the maximum entropy method for proposing a probability distribution based on the concept of information.

For a system S we can assign probabilities p_i to each possible state, and depending on the distribution of these probabilities we can infer the current state of the system with certain confidence. For instance, for a uniform distribution, we have the same probability for all the states, maximizing its uncertainty. Consequently, within information theory formalism we use the Shannon entropy for measuring this *amount* of information that we do not know about the system (see Eq. 3.7),

$$s = -\sum_i p_i \, log \, p_i. \tag{3.7}$$

In particular, for the uniform distribution, given that all the states are equally likely, their probabilities are given by $p_i = 1/N$ where N is the number of states, ans thus its entropy is equal to $logN$, while for a system whose probability distribution is for example a Dirac delta, we will obtain that the entropy is equal to zero. Consequently, we can understand this concept as a measurement of ignorance about the system. For instance, the thermodynamic equilibrium is the state which maximizes the entropy of the system.

Based on this concept, the maximum entropy method proposes a form of finding a probability distribution under the constraint of using the minimum information possible to describe the system, which is equivalent to maximizing the entropy. Thus, if we have information about one observable $\langle f(x) \rangle$ of a system s, the probability distribution is given by (see Appendix C):

$$p(x_i) = e^{-\lambda_1 - \lambda_2 f(x_i)} \tag{3.8}$$

Consequently, whether we have restricted information of the system, it is possible to use this probability distribution by adding the sufficient information coded on the observables $f(x_i)$ and Lagrange multipliers λ_i. Is is important to highlight that if we have n observables $f_n(x_i)$, we will have n Lagrange multipliers in this function.

Chapter 4

Results and analysis

As described in the preceding chapters, vision is one of the most studied sensory systems in vertebrates, and thus, knowledge about it is robust enough to understand quiet well its functioning. From a theoretical point of view, it is advantageous to study the visual system , given that there are real data to test any model or theory. In addition, the visual system is composed of structures such as the retina, whose anatomic structure is similar to that of the cortex, but with the advantage that the number of neurons is smaller, and consequently, is less complex. Some experimental works [51] [52] [53] on the vertebrate retina have been interpreted using statistical mechanics.

Since these experiments are the motivation for our work, the relevant results will be briefly presented in this section. Using the salamander retina as a biological sample[51], a set of 200 electrodes was implanted into the ganglion layer, to record the response of these cells under a continuous stimulus, during a period 2 hours. As is shown in the left panel of figure 4.1, the stimulus was a film of fish swimming in a natural environment, which was repeated for 2 hours. In addition, the figure shows the data collected in the experiment, containing the activity (spike or silence) of 120 cells.

The main purpose of these studies [51]-[53] was to propose a probability distribution by means of the maximum entropy criterion, aiming to construct an effective thermodynamics. The authors made a study of criticality using the formalism of equilibrium statistical mechanics, by defining effective quantities such as energy, entropy and temperature. The right panel of figure 4.1 shows the specific heat

curve, for different groups of neurons, whose peak at T=1 suggests that the retina could be at a critical point in this thermodynamic representation..

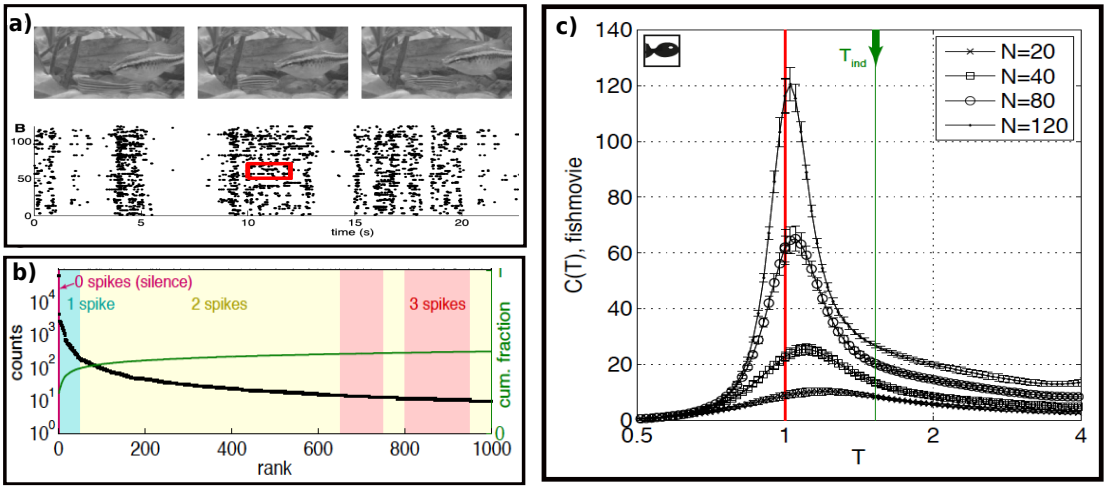

FIGURE 4.1: A) Above: three frames from the natural movie stimulus showing swimming fish and water plants. Below: The responses of a set of 120 neurons to a single stimulus repeat, black dots designate spikes. b) Number of occurrences of each pattern, with labels for the total number of spikes in each pattern. Taken from [52]. c) Heat capacity, C(T), computed for subnetworks of N =20; 40; 80; 120, neurons. Taken from [51]

The aim of our work is to use a similar treatment with data taken from the virtual retina software (see chapter 2 & Appendix A), testing if this system shows the same signs of criticality, under different stimuli.

4.1 Virtual retina parameters

The parameters of the virtual retina were configured following the same biological values used in the experiments described in subsection 2.4.1. Thus, in this section we will discuss these features and some computational characteristics of the simulation.

Unlike the vertebrate outer retina, the virtual outer retina contains just with one type of photoreceptor, given that the code structure does not make any functional or anatomical distinction among these neurons. In the case of the human retina, there are two types of photoreceptors: cones and rods, which are activated

depending on the intensity of light in the environment. For instance, when the stimuli ranges in the scotopic and mesopic region[1] of luminosity, the rods have their maximal activity, in contrast with the cones, whose activity maximizes in the photopic region. Consequently, since the film used in the experiments keeps the same luminance range, without sudden changes, we can assume that only one type of photoreceptor is activated, making feasible and realistic our simulation.

On the other hand, in some animals, such as primates [54], the arrangement of photoreceptors over the retina is not uniform, such that, the majority of cones are densely located in the fovea, and the majority of rods are distributed radially below the retinal pigment ephitellium. Therefore, if the size of the region analysed in the experiment is small enough (area of 200 ganglion cells), compared with the total retina size, (area of approximately 1 million ganglion cells) [55], the homogeneity of photoreceptor is plausible.

In the virtual inner retina, we used the same parameters used in the original paper[35] for simulating the contrast gain control, increasing the accuracy of the results compared with the real vertebrate retina observations, as was shown by the authors. Finally, as was already discussed, each animal species has a different classification of ganglion cells. In our simulations, we used the X and Y ganglion cells similar to those observed in cat's retinas, whose functional difference was already studied in chapter 2.

The simulator allows the modification of the ganglion layer, such that we are able to choose the type and number of cells we want to simulate. Therefore, besides the X and Y ganglion cells, we added two layers of ON and OFF cells for obtaining a structure of 4 sub-layers with each type of cells, for a total of 100 ganglion cells.

Concerning to the spatial distribution of photoreceptors, the virtual retina has the option of use a uniform square distribution or a radially decreasing distribution. In our case, despite the fact that we are simulating a vertebrate retina with complex spatial distribution, we chose the uniform square distribution, because of the small number of cells used. Finally, the parameters which describe the spatial and temporal filters in each layer were the same as were used in the original article

[1] By measuring the luminance of white paper in different environments, we find that the scotopic region is always below that of starlight, while the mesopic region ranges between that of starlight and the moonlight. The photopic range corresponds to luminance above that of moonlight.

[35], due to its similarity with the real vertebrate retina (for more details see Appendix A).

4.2 Simulations

The stimulus used in our simulation was the set of 55 images of 250 pixels used in the experiments of the original paper[35]. Each image is characterized by its intensity, ranging in a scale of 0 to 255, and the whole set represents a couple walking in a natural environment (see figure 4.2). In addition, for each image we used a characteristic processing time of $10ms$. Thus, the full set of images was repeated several times to reach 15 minutes of simulation. The signals of interest for our purposes come from the ganglion layer, thus, we collected the activity patterns of each individual ganglion cell, obtaining the data sets shown in figure 4.2.

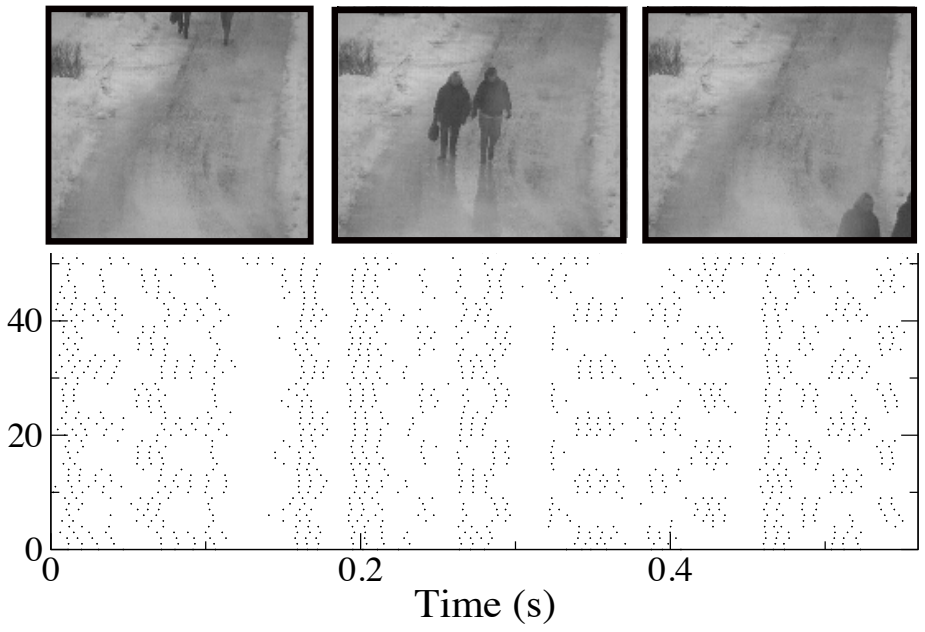

FIGURE 4.2: The stimulus used was a set of 56 images of 250 pixels, in grey scale, of a couple walking. In the upper part, we show three images presented at the beginning, the middle and the end of the whole film. The lower graph shows the activity of neurons (vertical axis) versus time (horizontal axis). This activity is presented in a binary way; silence (0) or activity (1).

For processing the data generated by the simulator, we defined the states of the system as a binary arrangement of length N, containing the information of the activity of each cell in a certain time bin. Given that the activity of the ganglion cells can be determined by the fact of having or not a spike, it is possible to simplify them as a two-level system, such that its state takes the value of 1 when spiking, and 0 otherwise. In our work we established the fixed bin of $2ms$, obtaining a total set of 3.4×10^5 states, which is comparable with the number of states analysed in the experimental work [52].

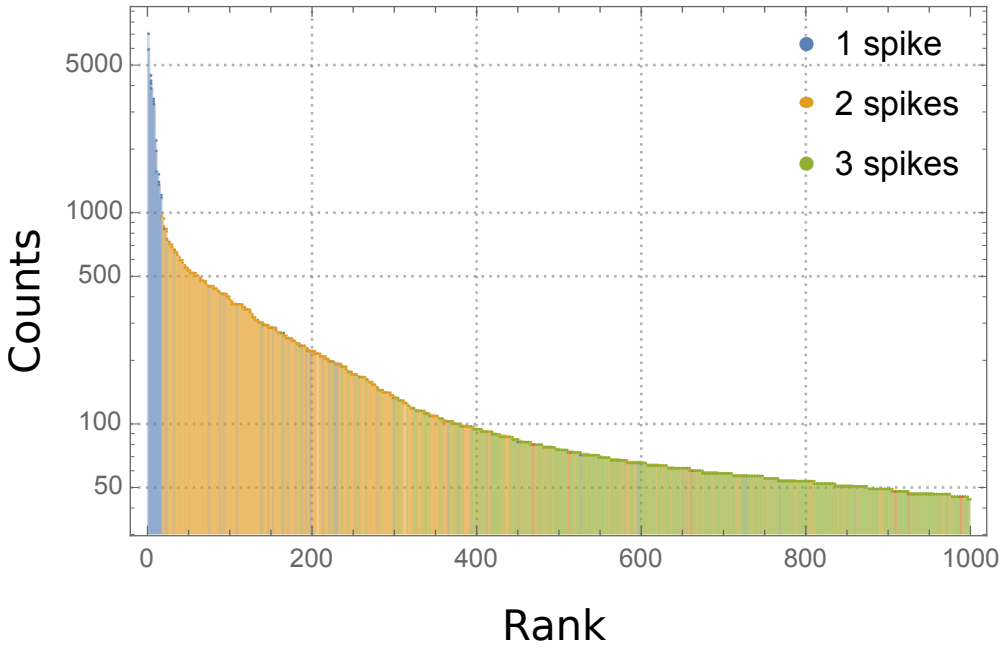

FIGURE 4.3: Number of occurrences of the 1000 most common patterns. The colors distinguish the patterns according to the number of cells spiking at the same time.

As expected from a biological viewpoint, most of the states found in the simulation are composed for less than 4 spikes i.e., 4 neurons in an active state at the same time, as shown in figure 4.3. These patterns are similar in the experiments with real retinas (see figure 4.1). One important fact in this treatment is that these states depend on the size of the bin; when the bin is large, the number of spikes per state increases and otherwise, decreases. Thus, in our work we used a similar bin used in the experimental works, which are based on real values of synchronized cells and in studies made with different bin sizes[2].

[2]Bialek. et.al. show that the general behaviour of the system does not change when the bin size is changed[52].

4.3 Maximum entropy model

Following the idea of the maximum entropy method discussed in chapter 3, we must propose a Hamiltonian using the minimal information possible to describe the probability distribution on the state space of the virtual retina. First, we must establish what is the relevant information that we can infer of the data for conserving the relevant features of the retina. Taking into account that the structure of our system is that of a network composed of neurons as nodes and synapses as links, we focus first on the mean behaviour of each individual neuron. We can write the states of each individual neuron as $\sigma_i = \{1, 0\}$, representing spike and silence respectively. Consequently the mean $\langle \sigma_i \rangle$ will range between 0 and 1, depending on the activity of the cell during the simulation.

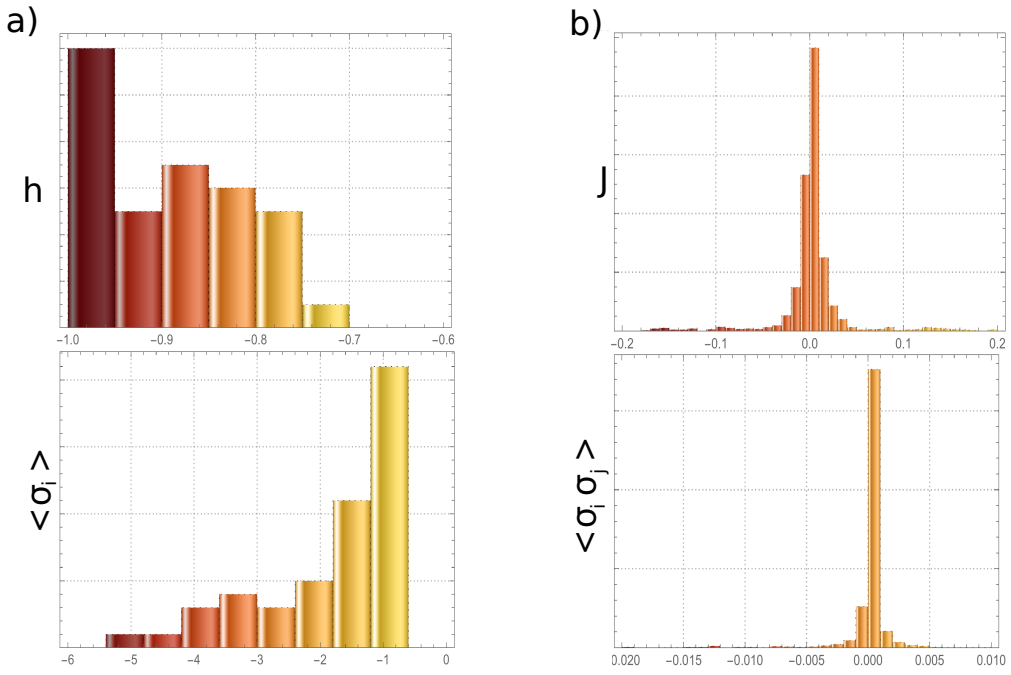

FIGURE 4.4: a) Distributions of variables h_i and means of each neuron σ_i. b) Distributions of variables J_{ij} and covariances $\sigma_i \sigma_j$

The second property that we must analyse is the interaction among these ganglion neuronsfor which, we will propose a pairwise interaction (like possible gapjuctions). It is clear that the interactions can involve more than two neurons at time, however following the discussions in [52] [56], these interactions can be neglected in the retina. Consequently, we will work only with pairwise interactions

aiming to capture the most important details of the real structure. Using the data of the simulation, we can extract this information using the covariances $\langle \sigma_i \sigma_j \rangle$.

Following this discussion and using the probability distribution of the maximum entropy formalism, we can define one Lagrange multiplier h_i related to the mean of each neuron and a set of pairwise interaction parameters J_{ij}, obtaining:

$$H = -\sum_i h_i \sigma_i - \sum_{ij} J_{ij} \sigma_i \sigma_j \tag{4.1}$$

Where h_i represents, in the real system, the weight of the external stimuli related with the intensity of the image and features of the cell itself, which in principle are different for each neuron, and J_{ij} represents the strength of the interaction between a pair of cells; the distribution of these variables are shown in figure 4.4. This Hamiltonian shares features with the Ising Hamiltonian (see Equation 3.3), with the difference that both the external field and the interaction constants, different for each neuron or pair of neuron. different for each neuron or pair of neurons. Note as well that J_{ij} is in general nonzero for any pair of neurons (interactions are not restricted to nearest neighbors), and that J_{ij} can take negative as well as positive values.

So far, we proposed a Hamiltonian aiming at describing the ganglion responses of the virtual retina. However, we do not have the values neither of the fields nor the interaction constants a priori; to find them, we use an inverse Monte-Carlo (MC) simulation. The next section is dedicated to describe the details of this simulation and some of its results.

4.4 Monte-Carlo Simulation

Taking into account that we have the energy of the system Eq. 4.1, we use the Metropolis method which is a type of Monte Carlo (MC) simulation The basic procedure followed by the routine is:

- Generate an initial guess for the h_i and J_{ij} as a set of independent random variables, by means of a uniform distribution.
- Choose a neuron i at random.

- If $\sigma_i = 0$ ($\sigma_i = 1$), change to $\sigma_i = 1$ ($\sigma_i = 0$), and calculate the energy change ΔE
- If $\Delta E < 0$, keep the new configuration. Otherwise, keep the new configuration just with a probability p_0, and with probability $1 - p_0$ retain the old configuration
- Repeat n_{mcs} times. In our simulations $n_{mcs} = 1 \times 10^6$.

Where the probability is given by $p_0 = exp\,[-\Delta E]$[16]. This routine generates a Markov chain in state space, allowing its analysis using statistical mechanics. Given that we do not know the parameters h_i and j_{ij} of the energy, we set an initial condition and start to *learn* the Hamiltonian for fitting the experimental observations.

By using the data generated with the virtual retina, which are referred to here as *experimental* data, we studied sub-systems of $9, 16, 25, 36$ and 49 neurons each. In general, for a system of size N, we selected its neurons randomly from the group of 100 neurons, and by means of the inverse MC we calculated the probability distribution. To improve our results, we repeated this process for 5 different subgroups of size N. Figure 4.5 shows the comparison of the means for subgroups of different sizes and Figure 4.6 shows the comparison of the covariances. We observe that the results fit the experimental observations.

Given that the energy is defined by N parameters h and $(N \times N)/2$ parameters J, we must adjust $N + (N \times N)/2$ parameters *at the same time*. Therefore, we used a gradient descent method for solving this minimization problem and adjust these parameters as:

$$h_i^{t+1} = h_i^t - \alpha\,[\langle\sigma_i\rangle_{exp} - \langle\sigma_i\rangle_{pre}] \tag{4.2}$$

$$J_{i,j}^{t+1} = J_{i,j}^t - \beta\,[\langle\sigma_i\sigma_j\rangle_{exp} - \langle\sigma_i\sigma_j\rangle_{pre}] \tag{4.3}$$

By increasing the MC steps for each simulation (more than 1×10^6), the accuracy of the results improves (error below 5%). Nevertheless the computational time becomes larger for the bigger subgroups decreasing the efficiency of the simulations.

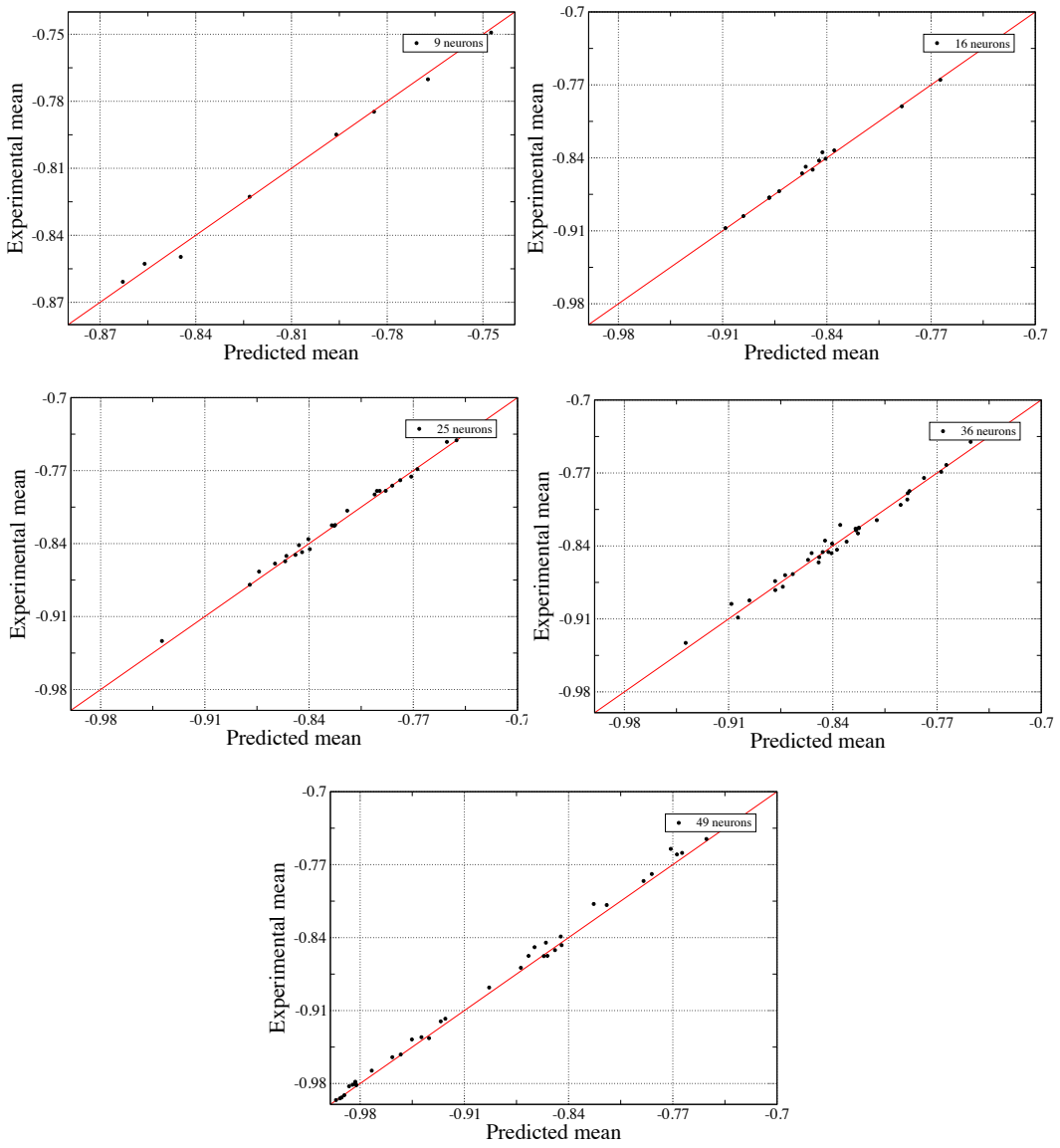

FIGURE 4.5: Comparison between the experimental and predicted means for groups of a) 9 neurons, b) 16 neurons, c) 25 neurons, d) 36 neurons and e) 49 neurons.

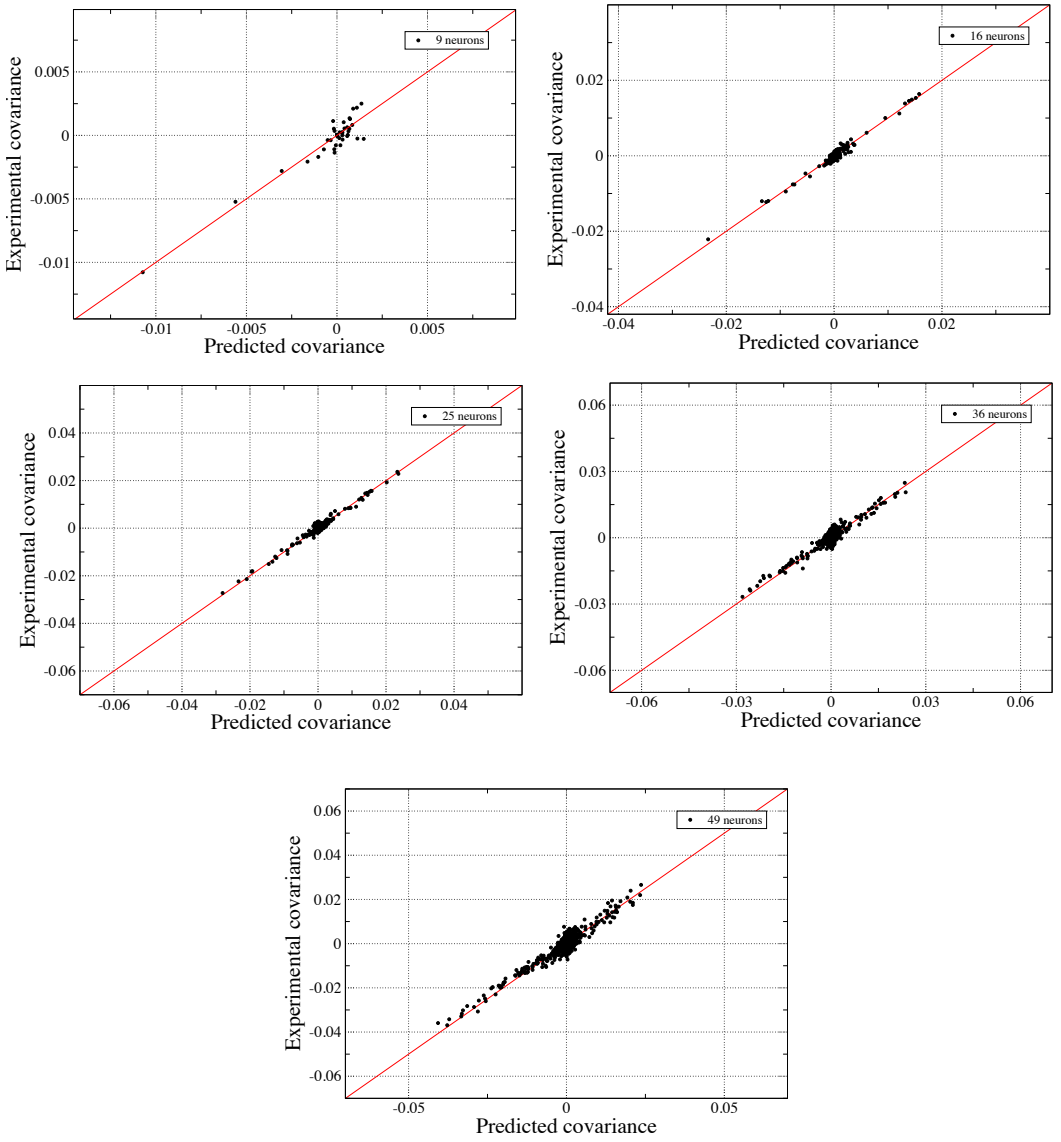

FIGURE 4.6: Comparison between the experimental and predicted covariances for groups of a) 9 neurons, b) 16 neurons, c) 25 neurons, d) 36 neurons and e) 49 neurons.

4.5 Thermodynamics

Following the discussion in chapter 3, we can propose a thermodynamics for the system by means of the inferred probability distribution (see Diagram 4.7). Comparing the mathematical form of the Boltzmann distribution (Equation 3.1) with the probability distribution of the maximum entropy theory, we note that the difference lies in the term $k_B T$, in which for $k_B = 1$, we would have just the temperature to be discussed. It is clear that the concept of temperature emerges from thermodynamics and is well understood in systems at equilibrium, however, we can define an effective temperature in our probability distribution in order to apply the formalism of equilibrium criticality,

$$p(\{\sigma_i\}) = exp\left(-\frac{H}{T_{eff}}\right). \tag{4.4}$$

In order to find signals of criticality in the system, we can follow the logic used in the analysis of the Ising model (see chapter 3), for which we calculated the specific heat for different temperatures, expecting a divergent behaviour near to the critical temperature T_c. Given that we have the probability distribution of the system we can calculate the specific heat of the system with different effective temperatures, expecting a kind of special behaviour near to $T_{eff} = 1$, which is the temperature of the system[3].

A was studied in chapter 3 and Appendix B, we can calculate the specific heat of a thermodynamic system by calculating the mean of the energies for a fixed temperature. Thus, by using equation Equation 3.5 we calculated the specific heat curve for each subgroup of N neurons and we calculated their mean value for constructing a general one. To obtain the mean over the energies, we made MC simulations to generate the states of the system and averaging over them. We repeated this procedure for several effective temperatures to obtain the curves shown in figure 4.8.

By looking at the temperature of the system $T = 1$, we observe a peak in the specific heat curve, increasing with the size of the system, and consequently suggesting a possible critical behaviour in this point. In chapter 3 we studied the

[3]Taking into account the Boltzmann distribution at $T = 1$ is equal than the maximum entropy distribution (with $k_B = 1$), we establish that our system works at $T_{eff} = 1$.

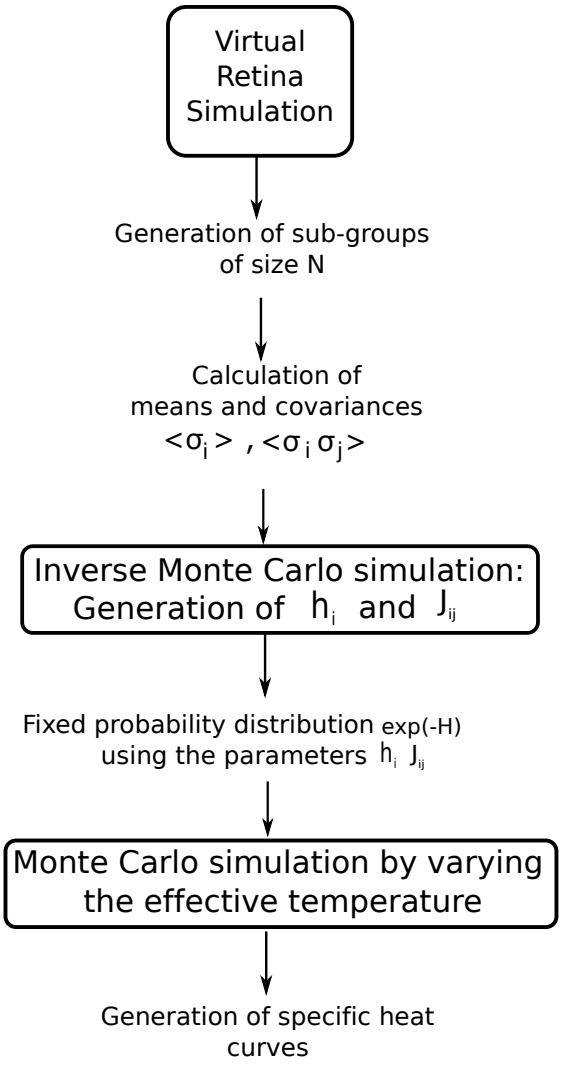

FIGURE 4.7: Diagram for describing the simulation steps.

behaviour of the Ising model in the critical point and we observed the same behaviour in this curve, thus, making a comparison, we think that this behaviour suggest a possible critical state in the virtual retina.

Concerning the experimental results, the virtual retina shows a similar behaviour in the specific heat curves, suggesting that this is not a singularity of the data, rather, a property of the biological system. In both experimental and simulation treatments, the temperature was an effective parameter interpreted as noise in the model, which means that the noise of the signal increases as far as the temperature drives off the system temperature $T = 1$. Nevertheless, in contrast

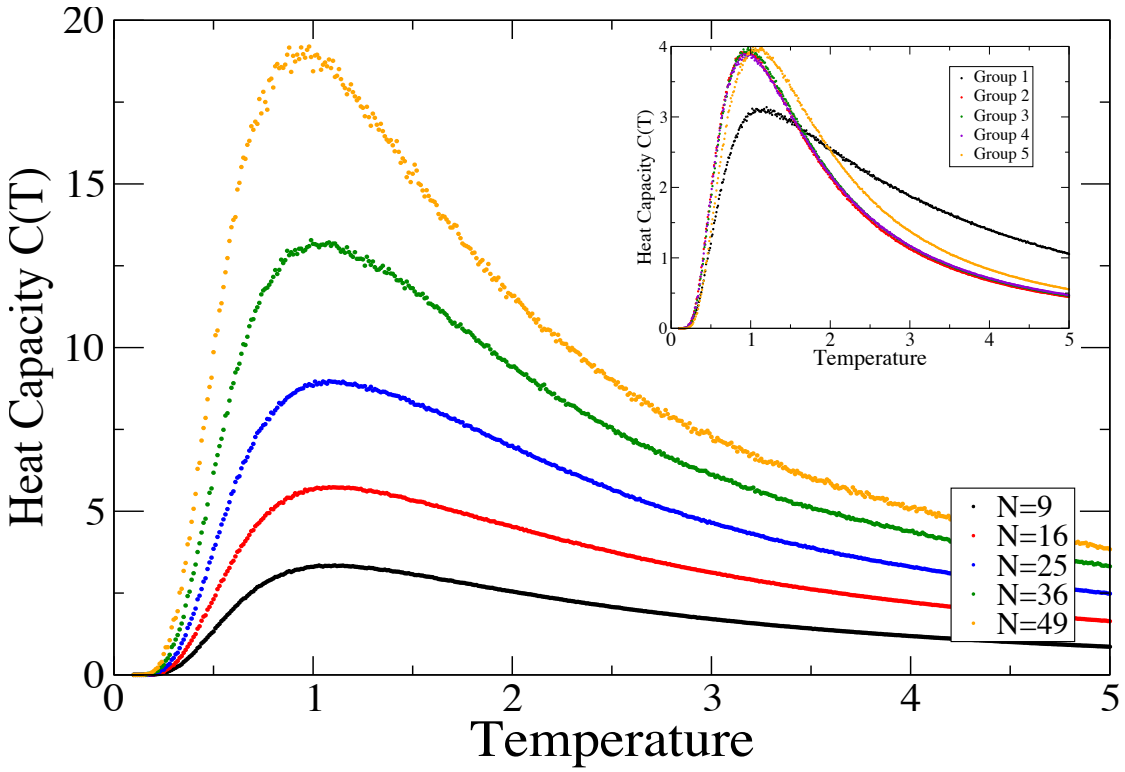

FIGURE 4.8: Specific heat for lattices of 9, 16, 25, 36 and 49 neurons. The inset shows the curves for the 5 groups of size N=9, from which we calculated the mean curve.

with equilibrium systems, in which these quantities have a direct physical meaning, in our system we must work on the interpretation of this possible critical state. For instance, if this critical state exist in real systems, *what would be its direct interpretation?* The non-equilibrium theories of criticality in the brain suggest that criticality appears physically as avalanches in the system helping to the optimization of the system (see discussion on chapter 3), thus, the motivation of finding these conceptual meaning for the effective variables used in our framework, is related with the understanding of this critical state and its relation with the non-equilibrium theories.

Chapter 5

Conclusions and perspectives

From a biological viewpoint, we can remark that the retina is a complex and important part in the visual system, processing the luminous stimuli. Its layered structure is similar of that in the cortex, making possible the comparison and extrapolation of results, with the advantage that the retina is smaller than the cortex, making feasible its study from a theoretical and experimental framework. By means of the virtual retina simulator we obtained data on the ganglion layer reproducing with good accuracy the observations in real vertebrate retinas and allowing the study of this biological system without the complications of real experiments. Therefore, we can conclude that it is possible to construct simulations with a reasonable computational cost for describing this network, aiming for find a kind of general behaviour that might be relevant to the entire brain.

By applying the maximum entropy method within the information theory framework, we found a probability distribution able to reproduce the most general features of the data, allowing the study of this system from the viewpoint of statistical mechanics. Thus, by describing each individual neuron within a brief time interval as a two-level system, we were able to find a mathematical function for describing some features of the data. However, it is important to highlight that these observables upon which we based our analysis, such as means and covariances, were chosen by intuition and non necessarily are of biological relevance.

Finally, searching for a kind of universality of these complex biological networks, we analysed the critical behaviour of the system from an equilibrium framework. As found in experiments on real retinas, we obtained signals of criticality by studying

the specific heat curves of the Ising model with parameters adjusted to reproduce firing-state probabilities, for different sizes of networks.

One of the perspectives of our work is related with the deep study of the virtual retina by using different stimulations. First, we will analyse the response of the virtual retina under a noisy pattern (independent dark and light pixels) aiming for finding differences in the correlations, and after, we will introduce some *critical* signals, such as configurations from both the 2-dimensional Ising model and sandpile, both at and away from criticality. In addition, we will introduce some variations on the parameters defining the virtual retina features, such as the spatial and temporal filters which describe the functional behaviour of the cells contained on each layer, in order to obtain a more general and robust conclusion.

Appendix A

Virtual retina

A.1 Dimensional analysis

For an individual neuron, the mathematical equation which describes the electric impulse is given by [20]:

$$c\frac{dV}{dt} = \sum_i I_i + \sum_j g_j(E_j - V) \tag{A.1}$$

To obtain a simpler dimensionless system, it is made a normalization of variables $V \to (V - V_R)/\Delta V$,$I \to I/c\Delta V$ and $g \to g/c$. Where c is the membrane capacity, ΔV is a typical range of variation for the neuron's potential and V_R is the resting potential, with the physiological values $c \equiv 0.1nF$ and $\Delta V \equiv 20mv$ taken from measurements in mammalian ganglion and bipolar cells [35].

A.2 Spatial and temporal filters

In order to describe in a computational way the spatial and temporal biological behaviour of the retina, the simulation is constructed on the basis of four main filters:

- **Exponential low-pass temporal filter**: This filter peaks at time τ, representing the characteristic time and the only free parameter.

$$E_\tau(t) = \frac{exp(\frac{-t}{\tau})}{\tau} \tag{A.2}$$

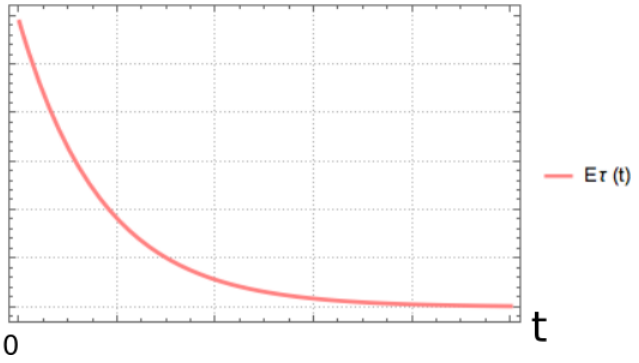

- **Exponential cascade low pass temporal filter**: This filter peaks at time τ and offers more variability in its shape because of the additional $n > 0$ parameter.

$$E_{n,\tau}(t) = (nt)^n \frac{exp(\frac{-nt}{\tau})}{(n-1)!\,\tau^{n+1}} \tag{A.3}$$

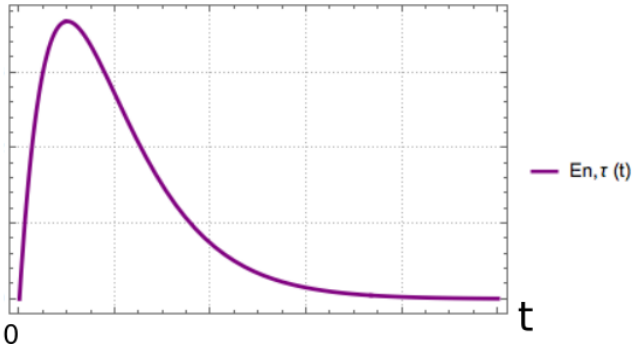

- **Partially high-pass temporal filter**: This filter is composed of two terms, such that, the first represents the original signal via the Dirac function, and the second removes the low-pass average, with a weight ω, using the exponential filter.

$$T_{\omega,\tau}(t) = \delta_0(t) - \omega E_\tau(t) \tag{A.4}$$

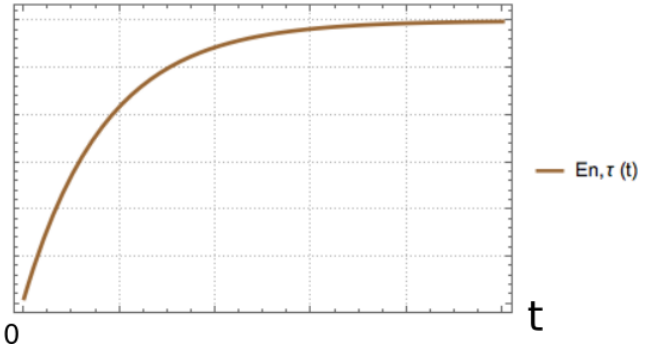

- **Low-pass spatial filter**: This filter is described as a two-dimensional Gaussian, characterized by its mean and variance.

$$G_\sigma(x,y) = \frac{exp(-\frac{x^2+y^2}{2\sigma^2})}{2\pi\sigma} \tag{A.5}$$

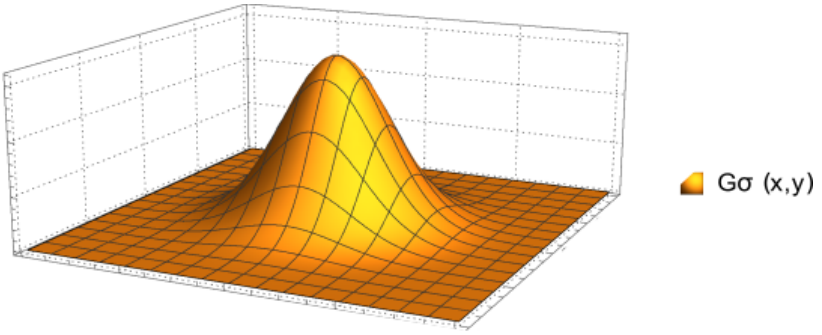

Appendix B

Specific heat and susceptibility

Using the partition function $Z = \sum_\zeta e^{-E_\zeta/K_BT}$ used in chapter 3, we can introduce the identity $\int dE\, \delta(E - E_s) = 1$ to obtain:

$$\begin{aligned} Z &= \int dE e^{-E/k_BT} \left[\sum_s (E - E_s) \right] \\ &= \int dE e^{-E/k_BT} n(E) \end{aligned}$$

Where $n(E)$ is the number of states with energy E. Taking into account that the integral of the delta function is equal to the step function, defined as:

$$\Theta(x) = \begin{cases} 1, & x > 0 \\ 0, & x < 0 \end{cases}$$

And integrating by parts, we can write the partition function in terms of the number of states $N(E)$ with energy in the interval $E \leq E_s$, which at the same time can be written in terms of the entropy Equation 3.2 as:

$$\begin{aligned} Z &= \frac{1}{k_BT} \int dE exp[-\frac{E}{k_BT}] N(E) \\ &= \frac{1}{k_BT} \int dE exp \left[-\frac{E}{k_BT} + S(E) \right] \end{aligned}$$

Therefore, from this equation we can define the free energy as $f(\epsilon) = \epsilon - k_B T s(\epsilon)$. In the thermodynamic limit we expect this quantity being minimized $\left(\frac{df(\epsilon)}{d\epsilon} = 0\right)$, which leads to the equation:

$$\frac{ds(\epsilon)}{d\epsilon} = \frac{1}{k_B T}$$

Thus, for $N \longrightarrow \infty$, we can use the Taylor expansion to write the partition function as:

$$Z \approx \frac{N}{k_B T} e^{-Nf(\epsilon^*)/k_B T} \int d\epsilon \, e^{-\frac{N}{2}\left[-\frac{d^2 s(\epsilon)}{d\epsilon^2}|_{\epsilon^*}\right](\epsilon-\epsilon^*)^2}$$

Comparing this result with a Gaussian distribution, we can write:

$$\begin{aligned} \langle \delta\epsilon \rangle &= \epsilon^* \\ \langle (\delta\epsilon)^2 \rangle &= \frac{1}{N}\left[-\frac{d^2 s(\epsilon)}{d\epsilon^2}\,|_{\epsilon^*}\right]^{-1} \end{aligned}$$

On the other hand, we can use the Boltzmann probability distribution to calculate the mean energy of the system, as:

$$\langle \delta\epsilon \rangle = \sum_{\zeta} \epsilon e^{-N\epsilon_\zeta / k_B T} / Z$$

Taking into account that the specific heat is defined as the energy change with respect to the temperature, we can write:

$$\begin{aligned} c_v = \frac{d\epsilon^*}{dT} &= \frac{d\langle \delta\epsilon \rangle}{dT} = \frac{\frac{d}{dT}\left[\sum_\zeta \epsilon e^{-N\epsilon_\zeta / k_B T}\right]}{Z} \\ &= \frac{N}{k_B T}\langle (\delta\epsilon)^2 \rangle \\ &= \frac{1}{k_B T}\left[-\frac{d^2 s(\epsilon)}{d\epsilon^2}\,|_{\epsilon^*}\right]^{-1} \end{aligned}$$

Since the magnetization is defined as $m = \sum_i \sigma_i$, its change in terms of the magnetic field is known as magnetic susceptibility. We use a similar treatment to find a useful expression for this quantity, nevertheless, in this case we use the Ising Hamiltonian with constant H and same interactions among spins. Thus, the result is not general for all systems.

Using Boltzmann distribution, we know that:

$$\langle m \rangle = \frac{\sum_n m e^{-\beta E_n}}{z} \tag{B.1}$$

Writing the free energy in terms of the partition function as $F(\epsilon) = -k_B T log(Z)$

Appendix C

Maximum entropy

For describing completely any system, we need the probabilities of each possible state p_i, such that we can calculate the means of all observables and predict its behaviour as:

$$\langle g(x) \rangle = \sum_{i}^{n} p_i g(x_i). \tag{C.1}$$

Nevertheless, for some systems we do not have this information, rather, we have just information about another observable $\langle f(x) \rangle$. *Is it possible to calculate the mean of the observable* $g(x)$ *in C.1 by using just the information of* $\langle f(x) \rangle$*?* It is clear that we need to infer more information about the system for solving this problem given that we have much more parameters $(n-1)$ than equations. Thus, *can we make some assumption about the probability distribution of the system?* the first attempt was made by Jaimes Bernoulli [57], who proposed the principle of *non-sufficient reason* [1] based on the idea that if for several arguments, there is absence of information to assign unequal probabilities, equal probabilities must be assigned to each one. However, this principle makes an arbitrary symmetry assumption that in principle do not must be valid in all systems[58].

The approach of the maximum entropy theory is based on minimize the information function of the system, such that we use just the sufficient information for describing the system. Thus, by using the Shannon entropy as a measurement of

[1] Known too as *Principle of indifference*

ignorance (see discussion in chapter 3) we can maximize it by including the constrain of the observable $\langle f(x)\rangle$ and the normalization condition for the probability $\sum_i p_i = 1$, by means of Lagrange multipliers:

$$F = -K\sum_i p_i \log p_i - \beta\left[\sum_i p_i f(x_i) - \langle f(x)\rangle\right] - \lambda\left[\sum_i p_i - 1\right] \tag{C.2}$$

Where K is a constant which we will define as $K = 1$, and β and λ are the Lagrange multipliers. By maximizing:

$$\begin{aligned} \frac{\delta F}{\delta p_i} &= -\log p_i - 1 - \beta f(x_i) - \lambda \\ \log p_i &= -1 - \beta f(x_i) - \lambda \\ p_i &= e^{-\lambda - \beta f(x_i)} \end{aligned} \tag{C.3}$$

Consequently, by maximizing the entropy we find this distribution of probability to describe the system under the assumption of minimal information.

Bibliography

[1] René Descartes and Et Gilson. *Discours de la méthode*. Vrin, 1987.

[2] Seiji Ogawa, Tso-Ming Lee, Alan R Kay, and David W Tank. Brain magnetic resonance imaging with contrast dependent on blood oxygenation. *Proceedings of the National Academy of Sciences*, 87(24):9868–9872, 1990.

[3] Peter G Morris. Nuclear magnetic resonance imaging in medicine and biology. 1986.

[4] JW Belliveau, DN Kennedy, RC McKinstry, BR Buchbinder, RMt Weisskoff, MS Cohen, JM Vevea, TJ Brady, and BR Rosen. Functional mapping of the human visual cortex by magnetic resonance imaging. *Science*, 254(5032): 716–719, 1991.

[5] Seong-Gi Kim, James Ashe, Kristy Hendrich, Jutta M Ellermann, Hellmut Merkle, Kamil Ugurbil, and Apostolos P Georgopoulos. Functional magnetic resonance imaging of motor cortex: hemispheric asymmetry and handedness. *Science*, 261(5121):615–617, 1993.

[6] Francisco López-Muñoz, Jesús Boya, and Cecilio Alamo. Neuron theory, the cornerstone of neuroscience, on the centenary of the nobel prize award to santiago ramón y cajal. *Brain research bulletin*, 70(4-6):391–405, 2006.

[7] John A Hertz. *Introduction to the theory of neural computation*. CRC Press, 2018.

[8] Jianfeng Feng. *Computational neuroscience: a comprehensive approach*. CRC press, 2003.

[9] Peter Dayan, LF Abbott, et al. Theoretical neuroscience: computational and mathematical modeling of neural systems. *Journal of Cognitive Neuroscience*, 15(1):154–155, 2003.

[10] Ariel Haimovici, Enzo Tagliazucchi, Pablo Balenzuela, and Dante R Chialvo. Brain organization into resting state networks emerges at criticality on a model of the human connectome. *Physical review letters*, 110(17):178101, 2013.

[11] Per Bak. *How nature works: the science of self-organized criticality*. Springer Science & Business Media, 2013.

[12] Charles F Richter. An instrumental earthquake magnitude scale. *Bulletin of the Seismological Society of America*, 25(1):1–32, 1935.

[13] Jens Feder. *Fractals*. Springer Science & Business Media, 2013.

[14] Miguel A Muñoz, Róbert Juhász, Claudio Castellano, and Géza Ódor. Griffiths phases on complex networks. *Physical review letters*, 105(12):128701, 2010.

[15] Paolo Moretti and Miguel A Muñoz. Griffiths phases and the stretching of criticality in brain networks. *Nature communications*, 4:2521, 2013.

[16] James Sethna. *Statistical mechanics: entropy, order parameters, and complexity*, volume 14. Oxford University Press, 2006.

[17] Dale Ed Purves, George J Augustine, David Ed Fitzpatrick, Lawrence C Katz, et al. *Neuroscience.* Sunderland, MA, US: Sinauer Associates, 1997.

[18] Maria A Patestas and Leslie P Gartner. *A textbook of neuroanatomy*. John Wiley & Sons, 2016.

[19] Richard S Snell. *Clinical neuroanatomy*. Lippincott Williams & Wilkins, 2010.

[20] Alan L Hodgkin and Andrew F Huxley. A quantitative description of membrane current and its application to conduction and excitation in nerve. *The Journal of physiology*, 117(4):500–544, 1952.

[21] Eric R Kandel, James H Schwartz, Thomas M Jessell, Steven A Siegelbaum, A James Hudspeth, et al. *Principles of neural science*, volume 4. McGraw-hill New York, 2000.

[22] Owen P Hamill, A Marty, Erwin Neher, Bert Sakmann, and FJ Sigworth. Improved patch-clamp techniques for high-resolution current recording from cells and cell-free membrane patches. *Pflügers Archiv*, 391(2):85–100, 1981.

[23] Mustafa BA Djamgoz, Hans-Joachim Wagner, and Paul Witkovsky. Photoreceptor-horizontal cell connectivity, synaptic transmission and neuromodulation. In *Neurobiology and clinical aspects of the outer retina*, pages 155–193. Springer, 1995.

[24] Mark W Hankins. Horizontal cell coupling and its regulation. In *Neurobiology and Clinical Aspects of the Outer Retina*, pages 195–220. Springer, 1995.

[25] Steven Barnes. Photoreceptor synaptic output: neurotransmitter release and photoreceptor coupling. In *Neurobiology and clinical aspects of the outer retina*, pages 133–153. Springer, 1995.

[26] Helga Kolb and Ralph Nelson. The organization of photoreceptor to bipolar synapses in the outer plexiform layer. In *Neurobiology and clinical aspects of the outer retina*, pages 273–296. Springer, 1995.

[27] MBA Djamgoz, L Spadavecchia, C Usai, and S Vallerga. Variability of light-evoked response pattern and morphological characterization of amacrine cells in goldfish retina. *Journal of comparative neurology*, 301(2):171–190, 1990.

[28] Barry B Lee. Problems posed by primate ganglion cells for functional anatomy and psychophysics. In *Neurobiology of the Inner Retina*, pages 389–400. Springer, 1989.

[29] Robert Shapley and V Hugh Perry. Cat and monkey retinal ganglion cells and their visual functional roles. *Trends in Neurosciences*, 9:229–235, 1986.

[30] Christina Enroth-Cugell and John G Robson. The contrast sensitivity of retinal ganglion cells of the cat. *The Journal of physiology*, 187(3):517–552, 1966.

[31] Justin Keat, Pamela Reinagel, R Clay Reid, and Markus Meister. Predicting every spike: a model for the responses of visual neurons. *Neuron*, 30(3): 803–817, 2001.

[32] Matthias H Hennig, Klaus Funke, and Florentin Wörgötter. The influence of different retinal subcircuits on the nonlinearity of ganglion cell behavior. *Journal of Neuroscience*, 22(19):8726–8738, 2002.

[33] JH van van Hateren, L Rüttiger, H Sun, and BB Lee. Processing of natural temporal stimuli by macaque retinal ganglion cells. *Journal of Neuroscience*, 22(22):9945–9960, 2002.

[34] Jeanny Hérault and Barthélémy Durette. Modeling visual perception for image processing. *Computational and ambient intelligence*, pages 662–675, 2007.

[35] Adrien Wohrer and Pierre Kornprobst. Virtual retina: a biological retina model and simulator, with contrast gain control. *Journal of computational neuroscience*, 26(2):219–249, 2009.

[36] IZUMI Ohzawa, GARY Sclar, and RALPH D Freeman. Contrast gain control in the cat's visual system. *Journal of neurophysiology*, 54(3):651–667, 1985.

[37] Matteo Carandini, Jonathan B Demb, Valerio Mante, David J Tolhurst, Yang Dan, Bruno A Olshausen, Jack L Gallant, and Nicole C Rust. Do we know what the early visual system does? *Journal of Neuroscience*, 25(46):10577–10597, 2005.

[38] EJ Chichilnisky. A simple white noise analysis of neuronal light responses. *Network: Computation in Neural Systems*, 12(2):199–213, 2001.

[39] Peter Dayan and Laurence F Abbott. *Theoretical neuroscience*, volume 806. Cambridge, MA: MIT Press, 2001.

[40] Dennis M Dacey and Michael R Petersen. Dendritic field size and morphology of midget and parasol ganglion cells of the human retina. *Proceedings of the National Academy of sciences*, 89(20):9666–9670, 1992.

[41] Howard H Pattee. Hierarcht theorythe challenge of complex systems. Technical report, 1973.

[42] J. Marro and R. Dickman. *Nonequilibrium Phase Transitions in Lattice Models*. Collection Alea-Saclay: Monographs and Texts in Statistical Physics. Cambridge University Press, 2005. ISBN 9780521019460.

[43] Enrico Fermi THERMODYNAMICS. Unabridged reproduction of 1937 edition. *Elementary in*.

[44] Walter Greiner, Ludwig Neise, and Horst Stöcker. *Thermodynamics and statistical mechanics*. Springer Science & Business Media, 2012.

[45] Radu Balescu. Equilibrium and nonequilibrium statistical mechanics. *NASA STI/Recon Technical Report A*, 76, 1975.

[46] Birger Bergersen Michael Plischke. *Equilibrium Statistical Physics*. World Scientific Publishing Company, 2nd edition, 1994. ISBN 9789810216429,9789810248123,9810216424. URL http://gen.lib.rus.ec/book/index.php?md5=582D91D7ACB1B9E880F951B72B4D59B0.

[47] Lars Onsager. Crystal statistics. i. a two-dimensional model with an order-disorder transition. *Phys. Rev.*, 65:117–149, Feb 1944. doi: 10.1103/PhysRev.65.117. URL https://link.aps.org/doi/10.1103/PhysRev.65.117.

[48] Leo P Kadanoff. Scaling and universality in statistical physics. *Physica A: Statistical Mechanics and its Applications*, 163(1):1–14, 1990.

[49] Géza Ódor. Universality classes in nonequilibrium lattice systems. *Reviews of modern physics*, 76(3):663, 2004.

[50] Jean-Philippe Bouchaud and Marc Mézard. Universality classes for extreme-value statistics. *Journal of Physics A: Mathematical and General*, 30(23): 7997, 1997.

[51] Gašper Tkačik, Thierry Mora, Olivier Marre, Dario Amodei, Stephanie E Palmer, Michael J Berry, and William Bialek. Thermodynamics and signatures of criticality in a network of neurons. *Proceedings of the National Academy of Sciences*, 112(37):11508–11513, 2015.

[52] Gašper Tkačik, Olivier Marre, Dario Amodei, Elad Schneidman, William Bialek, and Michael J Berry II. Searching for collective behavior in a large network of sensory neurons. *PLoS computational biology*, 10(1):e1003408, 2014.

[53] Gasper Tkacik, Elad Schneidman, II Berry, J Michael, and William Bialek. Ising models for networks of real neurons. *arXiv preprint q-bio/0611072*, 2006.

[54] Wallace B. Thoreson. *The Vertebrate Retina*, pages 123–134. Springer US, Boston, MA, 2008. ISBN 978-0-387-72573-4. doi: 10.1007/978-0-387-72573-4_11. URL https://doi.org/10.1007/978-0-387-72573-4_11.

[55] Christine A Curcio, Kenneth R Sloan, Robert E Kalina, and Anita E Hendrickson. Human photoreceptor topography. *Journal of comparative neurology*, 292(4):497–523, 1990.

[56] Elad Schneidman, Michael J Berry II, Ronen Segev, and William Bialek. Weak pairwise correlations imply strongly correlated network states in a neural population. *Nature*, 440(7087):1007, 2006.

[57] John Maynard Keynes. A treatise of probability. *Phil. Trans*, 53:376–398, 1763.

[58] Edwin T Jaynes. Information theory and statistical mechanics. *Physical review*, 106(4):620, 1957.